Representing methane emissions from wet tropical forest soils using microbial functional groups constrained by soil diffusivity

Debjani Sihi[1,2], Xiaofeng Xu[3], Mónica Salazar Ortiz[4], Christine S. O'Connell[5,6], Whendee L. Silver[5], Carla López-Lloreda[7], Julia M. Brenner[1], Ryan K. Quinn[1,8], Jana R. Phillips[1], Brent D. Newman[9], and Melanie A. Mayes[1]*

[1]Climate Change Science Institute and Environmental Sciences Division, Oak Ridge National Laboratory, Oak Ridge, TN, 37831, USA
[2]Currently employed at Department of Environmental Sciences, Emory University, Atlanta, GA, 30322, USA
[3]Department of Biology, San Diego State University, San Diego, CA, 92182-4614, USA
[4]Institute of Plant Science and Microbiology, University of Hamburg, Hamburg, 20148, Germany
[5]Department of Environmental Science, Policy and Management, University of California, Berkeley, CA, 94720-3114, USA
[6]Currently employed at Department of Environmental Studies, Macalester College, St. Paul, MN, 55105-1899, USA
[7]Department of Natural Resources and the Environment, University of New Hampshire, Durham, NH, 03824, USA
[8]Department of Biology, Boston University, Boston, MA, 02215, USA
[9]Earth and Environmental Sciences Division, Los Alamos National Laboratory, Los Alamos, NM, 87545, USA

*Correspondence to: Melanie A. Mayes (mayesma@ornl.gov)

Abstract. Tropical ecosystems contribute significantly to global emissions of methane (CH_4) and landscape topography influences the rate of CH_4 emissions from wet tropical forest soils. However, extreme events such as drought can alter normal topographic patterns of emissions. Here we explain the dynamics of CH_4 emissions during normal and drought conditions across a catena in the Luquillo Experimental Forest, Puerto Rico. Valley soils served as the major source of CH_4 emissions in a normal precipitation year (2016), but drought recovery in 2015 resulted in dramatic pulses in CH_4 emissions from all topographic positions. Geochemical parameters including dissolved organic carbon (C), acetate, and soil pH; and hydrological parameters like soil moisture and oxygen (O_2) concentrations, varied across the catena. During the drought, soil moisture decreased in the slope and ridge and O_2 concentrations increased in the valley. We simulated the dynamics of CH_4 emissions with the Microbial Model for Methane Dynamics-Dual Arrhenius and Michaelis Menten (M3D-DAMM) which couples a microbial functional group CH_4 model with a diffusivity module for solute and gas transport within soil microsites. Contrasting patterns of soil moisture, O_2, acetate, and associated changes in soil pH with topography regulated simulated CH_4 emissions, but emissions were also altered by rate-limited diffusion in soil microsites. Changes in simulated available substrate for CH_4 production (acetate, CO_2, and H_2) and oxidation (O_2 and CH_4) increased the predicted biomass of methanotrophs during the drought event and methanogens during drought recovery, which in turn affected net emissions of CH_4. A variance-based sensitivity analysis suggested that parameters related to aceticlastic methanogenesis and methanotrophy were most critical to simulate net CH_4 emissions. This study enhanced the predictive capability for CH_4 emissions associated with complex topography and drought in wet tropical forest soils.

1 Introduction

43   Wet tropical forest soils contribute significantly to global emissions of methane (CH_4; Pachauri et al., 2014).

44   Although net emissions of CH_4 from upland soils are infrequent in temperate climates, studies show that CH_4

45   emissions are common in wet tropical forests, even in upland soils (Cattânio et al., 2002; Keller and Matson, 1994;

46   Silver et al., 1999; Teh et al., 2005; Verchot et al., 2000). Landscape topography can strongly influence the

47   proportions of CH_4 production and oxidation in mountainous tropical regions, affecting net emissions (Silver et al.,

48   1999; O'Connell et al., 2018). Climate, and specifically patterns in rainfall, also affect emissions from tropical

49   forests. Climate change may increase the frequency and severity of extreme rainfall and drought events, altering the

50   spatial and temporal dynamics of CH_4 emissions through changes in redox dynamics and substrate availability

51   (Silver et al., 1999; Chadwick et al., 2016; Neelin et al., 2006). Thus, accurately estimating CH_4 emissions under a

52   variety of climatic and topographic conditions is important for predicting soil carbon-climate feedbacks in the humid

53   tropical biome.

54   Several studies have reported the effect of drought events on biogenic CH_4 emissions across different wet tropical

55   forest soils. For example, Aronson et al. (2019) demonstrated that the lower soil moisture conditions during 2015-16

56   El Niño event increased consumption of atmospheric CH_4 in a wet tropical forest Oxisol of Costa Rica. Similarly, a

57   large-scale, 5-year throughfall exclusion experiment in a moist tropical forest Oxisol in Brazil also reported

58   increased consumption of atmospheric CH_4 under the drought treatment, followed by a recovery of CH_4 emissions to

59   pre-treatment values after the experiment ceased (Davidson et al., 2004, 2008). Using rainout shelters, Wood and

60   Silver (2012) found spatial variability in CH_4 oxidation rates, with an increase of 480% uptake in valleys in an

61   Ultisol in Puerto Rico. More recently, in a similar Puerto Rico Ultisol, O'Connell et al. (2018) reported increasing

62   consumption of atmospheric CH_4 during a Caribbean drought event, followed by increased production of CH_4 after

63   the drought was over. The post-drought net CH_4 emission rates were higher than the pre-drought emissions, such

64   that the benefits to atmospheric radiation imparted by the lowered emissions during the drought were eliminated.

65   The sharp differences between pre- and post-drought emissions suggested that drought affected the balance of

66   methanogenesis and methanotrophy in the soils, but the study lacked analysis of the microbial community's

67   contributions to these two separate processes.

68   The concept of "microsites" inside soil aggregates or within soil micropores can help explain the coexistence of

69   oxidative and reductive processes in soils (Silver et al., 1999; Teh and Silver, 2006), which may have occurred in the

70   post-drought period in the O'Connell et al. (2018) study. Oxygen can remain inside micropores during saturated

71   conditions and thereby maintain aerobic microbial respiration; likewise, hypoxic conditions can persist in microsites

72   under extended droughts and thereby maintain anaerobiosis. Additionally, liquid substrates for methanogenesis such

73   as acetate can accumulate in microsites under dry conditions because their diffusion to hungry microbial

74 communities may be restricted. Conversely, gaseous substrates such as CO_2 and H_2 may accumulate in microsites

75 under saturated conditions because gaseous diffusion can be limited. The observed rapid flush of CH_4 in response to

76 a post-drought wetting event (O'Connell et al., 2018) suggests methanogenesis continued during the drought in the

77 Ultisol's microsites, despite low soil moisture and high O_2 supply (Andersen et al., 1998; Bosse and Frenzel, 1998;

78 Teh et al., 2005; von Fischer and Hedin, 2002). Finely-textured soils common to the humid tropics can facilitate the

79 co-existence of reduced solute and gas species with O_2 because the rate of solute and gaseous exchanges is

80 controlled by diffusion into and out of microaggregates (Hall and Silver, 2013; Liptzin et al., 2010; Silver et al.,

81 2013). In particular, hematite precipitation on clay minerals, found in both Oxisols and Ultisols, can enhance

82 formation of soil aggregates because of their high surface area and charge properties (Hall et al., 2016). Soil organic

83 matter can also enhance aggregation and at the same time consume O_2 (Six et al., 2004). However, few if any

84 measurements of microsites exist in real field soils.

85 To explain the diverse observations of CH_4 emissions during and after drought across a wet tropical forest catena,

86 we hypothesized that explicit representations of diffusion into and out of microsites for gas and solute transport

87 would be required. To account for the balance of methanotrophy and methanogenesis, separate microbial functional

88 groups for CH_4 production and oxidation would need to be defined. Therefore, a microbial functional group model

89 for CH_4 production and consumption (Xu et al., 2015) was merged with a soil diffusivity module (Davidson et al.,

90 2012; Sihi et al., 2018) to simulate the dynamics of net *in situ* CH_4 emissions from soil microsites (Sihi et al.,

91 2020a). This module considers three key mechanisms for CH_4 production and consumption: aceticlastic

92 methanogenesis (production from acetate) and hydrogenotrophic methanogenesis (production from H_2 and CO_2), and

93 aerobic methanotrophy (oxidation of CH_4 and reduction of O_2) (Fig. 1). Here we report a modeling experiment to

94 explain contrasting patterns of observed CH_4 emissions following a severe drought in 2015 and we provide new data

95 to describe CH_4 emissions under non-drought conditions in 2016. We explicitly account for changes in soil

96 moisture, O_2, acetate, and microbial functional group dynamics within soil microsites in the model.

2 Materials and methods

2.1 Study site

99 The study was conducted across a tropical forest catena near the El Verde Research Station in the Luquillo

100 Experimental Forest (LEF) in northeastern Puerto Rico in the United States (Latitude 18°19'16.83" N, Longitude

101 65°49'10.13" W). The site is part of a National Science Foundation Long-Term Ecological Research (LTER) and

102 Critical Zone Observatory (CZO) site and is also part of the U.S. Department of Energy's Next Generation

103 Ecosystem Experiment-Tropics. The mean annual temperature at the site is 23 °C and the long-term mean rainfall is

104 approximately 3500 mm yr^{-1} with low seasonality (Scatena, 1989). Inter-annual variability of rainfall ranges

105 between 2600 mm yr^{-1} to 5800 mm yr^{-1}, sometimes associated with extreme rainfall events (approximately 100 mm

106 day^{-1}) from Caribbean storm systems (Heartsill-Scalley et al., 2007). The LEF is classified as a wet tropical forest

107 according to the Holdridge life zone system, which considers rainfall, elevation, latitude, humidity, and

108 evapotranspiration (Harris et al., 2012).

109 The landscape at the field site is highly dissected with short catenas, characterized by a land surface distance of < 30
110 m from ridgetop to valley (O'Connell et al., 2018). This study partitioned sampling along a catena from ridgetop,
111 slope, and valley topographic positions (Fig. S1). The soils are clay-rich Ultisols, which were derived from basaltic
112 and andesitic volcanoclastic parent materials. Soils are acidic (average pH is 4.3 and 5.1 in ridge and valley
113 topographic positions, respectively, Fig. 2). The valley soils have approximately 30% clay and approximately 15%
114 sand, while the ridge soils have approximately 22% clay and approximately 30% sand (Brenner et al., 2019). The
115 soils contain high concentrations of iron (Fe) and aluminum (Al) (oxy)hydroxides where their relative
116 concentrations vary along the catena and differences in Fe speciation are associated with variable redox conditions
117 (Hall and Silver, 2013, 2015). A detailed soil survey in the immediate vicinity lists three soil types (Zarzal, Cristol,
118 and Prieto) with a minimal litter layer due to rapid decomposition (Parton et al. 2007, Cusack et al. 2009), surface
119 (A) horizons 5 cm thick, and B horizons of 130 to 150 cm thick (Soil Survey Staff, 1995). The surface soil bulk
120 density ranged from 0.5 to 0.7 g cm^{-3}, and by 25 cm depth was 0.8 to 1.1 g cm^{-3} (Cabugao et al., in press), similar to
121 previous observations (Johnson et al., 2014; Silver et al., 1999). The forest composition is relatively diverse with the
122 mature Tabonuco (*Dacryodes excelsa* Vahl) and Sierra palm (*Prestoea montana*) trees being most dominant
123 (Scatena and Lugo, 1995; Wadsworth et al., 1951).

124 **2.2 Soil and porewater sampling**

125 Previous CH_4 measurements in the LEF at the soil surface, 10 cm depth, and 35 cm depth, found the highest CH_4
126 concentrations at 10 cm depth (Silver et al. 1999), while 30 cm depth was the location of maximum soil organic
127 carbon (SOC) concentrations (Johnson et al., 2014). To initialize the model, soil and soil water samples were
128 collected from depths ranging from 0 to 30 cm in accordance with these previous studies. Soil samples were
129 collected in triplicate from a depth of 0-10 cm and on a quarterly timeframe from the ridgetop, slope, and valley
130 positions for over two years. The soil pH was determined using a 1:2 ratio of soil:solution using a glass electrode
131 with 0.005 M $CaCl_2$ as the equilibrated soil solution (Thomas, 1996; Sihi et al. 2020b). Porewater samples were
132 collected approximately weekly for over two years using macro-rhizon soil water samplers (length = 5 cm)
133 (Rhizosphere Research Products B.V.; Wageningen, The Netherlands) installed at both 5-10 cm and 25-30 cm depth
134 in triplicate in the ridge, slope, and valley topographic positions (Sihi et al., 2020c). The soil water samples were
135 analyzed for organic acid concentrations (acetate) using High Performance Liquid Chromatography (Dionex ICS-
136 5000+ Thermo-Fisher Waltham, MA, USA) with the Dionex IonPac AS11-HC column using a potassium hydroxide
137 eluent and gradient elution. The samples were analyzed for total dissolved organic carbon (DOC) using a Shimadzu
138 total organic C analyzer (Shimadzu TOC-L CSH/CSN Analyzer Baltimore, MD, USA). The soil and porewater
139 measurements were conducted in 2017-2018 (the number of samples n ranged between 20 to 35, Fig. 2) to initialize
140 different model parameters for the catena, because measurements were not available for 2015-2016. To that end, the
141 chemical data were used as the reference characteristics of the bulk soil, and the temporal evolution of DOC, acetate,
142 and soil pH at the microsites were calculated using probability distributions of soil moisture and O_2 across soil
143 microsites over the two-year measurement window. Soil bulk density and particle density values were taken from
144 O'Connell et al. (2018).

2.3 In situ methane flux and soil driver measurements

Campbell Scientific CS 655 soil moisture and temperature sensors and Apogee SO-110 O_2 sensors were co-located with soil gas flux chambers at 15 cm soil depth along the catena, each with five replications along five transects (Fig. S1) (O'Connell et al., 2018). Following Liptzin et al. (2011), soil O_2 sensors were installed in gas-permeable soil equilibration chambers (295 cm^3). Data from these sensors were collected hourly using Campbell Scientific CR10000 data loggers and AM16/32B multiplexers (Campbell Scientific, Logan, UT, USA), which were processed using site-based calibration equations.

Soil flux chambers were placed on the top of the soil surface. Soil CH_4 emissions along the catena were measured during 2015 (February 26 to December 23, O'Connell et al., 2018; Silver, 2018) and 2016 (April 5 to July 18) (Sihi et al., 2020d) using a Cavity Ring-Down Spectroscopy gas analyzer (Picarro G2508, Santa Clara, CA, USA) connected to 12 automated eosAC closed dynamic soil chambers (Pumpanen et al., 2004) using a multiplexer (Eosense Inc., Dartmouth, Nova Scotia, Canada). Data for soil CH_4 emissions were processed using eosAnalyze-AC (v3.5.0) software followed by a series of quality control protocols (O'Connell et al., 2018). We used daily average values of drivers (soil temperature, soil moisture, and O_2 concentrations) and CH_4 emissions in the modeling exercise. See O'Connell et al (2018) for more information on the soil sensor, chamber arrays, and the data analysis pipeline.

The data from the 2015 Caribbean drought was partitioned into four distinct periods (O'Connell et al., 2018): (1) pre-drought from day of year (DOY) 57 to 115 (dark gray on Fig. 3), (2) the drought from DOY 116 to 236 (medium gray on Fig. 3), (3) drought recovery from DOY 237 to 328 (light gray on Fig. 3), and (4) post-drought from DOY 329 to 354 (white on Fig. 3). Total precipitation during the drought period was 700 mm in 2015 and 1088 mm during the same time frame in 2016 (Meteorological data from El Verde Field Station: NADP Tower, available at https://luq.lter.network/data/luqmetadata127).

2.4 Modelling approach

2.4.1 Microbial functional group model for methane production and oxidation

An existing microbial functional group-based model for CH_4 production and consumption (Xu et al., 2015) was adopted for this research (Sihi, 2020). As shown in Fig. 1, acetate and H_2/CO_2 represent substrate [Substrate$_{func_i}$] (nM cm^{-3}) for aceticlastic and hydrogenotrophic methanogenesis reactions, respectively. On the other hand, CH_4 and O_2 concentrations represent substrate for the methanotrophy reaction. Acetate and CO_2 are inputs based on measurements of soil water and pH described in Section 2.2. In the model, acetate is formed by fermentation and by homoacetogenesis (but not by syntrophic acetate oxidation) as defined in Xu et al. (2015) in their Appendix in Eq. A15 and A16 (Fig. 1b). Methylotrophic methanogenesis (Narrowe et al. 2019) is neglected in the model. The overall reaction rates are represented as:

$$\text{Reaction}_{rate_i} = \text{Biomass}_{func_i} \times \frac{\text{GrowR}_{func_i}}{\text{Efficiency}_{func_i}} \times \frac{[\text{Substrate}_{func_{1\ldots n}}]}{[\text{Substrate}_{func_{1\ldots n}}] + \text{KM}_{func_{1\ldots n}}} \times f(T) \times f(pH) \qquad (1)$$

178 where $\text{Reaction}_{\text{rate}_i}$ (in nM cm^{-3} hr^{-1}) is rate of CH$_4$ production and/or consumption under variable substrate

179 concentrations. $\text{Biomass}_{\text{func}_i}$ (nM cm^{-3}) represents microbial functional groups: aceticlastic methanogens,

180 hydrogenotrophic methanogens, and aerobic methanotrophs, respectively. Growth rates and substrate use

181 efficiencies of microbial functional groups are represented as $\text{GrowR}_{\text{func}_i}$(hr^{-1}) and $\text{Efficiency}_{\text{func}_i}$ (unitless),

182 respectively (Table 1). The substrate limitation on CH$_4$ production is imposed by assuming a Michaelis-Menten

183 relationship with the half-saturation constants for CH$_4$ production and oxidation being $\text{KM}_{\text{func}_{1\ldots n}}$ (nM cm^{-3}).

184 Although minor contributions of iron dependent anaerobic CH$_4$ oxidation to net CH$_4$ emissions can be expected in

185 our study site (Ettwig et al., 2016), we did not represent this process here as anaerobic oxidation of CH$_4$ is still not

186 fully understood and it is generally low in most ecosystems.

187 The extent of change in $\text{Biomass}_{\text{func}_i}$ ($\text{dBiomass}_{\text{func}_i}$) is controlled by the balance between $\text{Growth}_{\text{func}_i}$ and

188 $\text{Death}_{\text{func}_i}$ following:

189 $$\frac{\text{dBiomass}_{\text{func}_i}}{\text{dt}_{\text{func}_i}}=\text{Growth}_{\text{func}_i} - \text{Death}_{\text{func}_i} \tag{2}$$

190 $$\text{Growth}_{\text{func}}=\text{Efficiency}_{\text{func}_i} \times \text{Reaction}_{\text{rate}_i} \tag{3}$$

191 where $\text{Growth}_{\text{func}_i}$ is calculated as a multiplicative function of $\text{Efficiency}_{\text{func}_i}$ and the $\text{Reaction}_{\text{rate}_i}$,

192 $$\text{Death}_{\text{func}_i}=\text{DeadR}_{\text{func}_i} \times \text{Biomass}_{\text{func}_i} \tag{4}$$

193 and $\text{Death}_{\text{func}_i}$ is a function of $\text{DeadR}_{\text{func}_i}$ (death rate, Table 1) and $\text{Biomass}_{\text{func}_i}$ (microbial biomass).

194 All rate equations were modified by the scalers for temperature, f(T) and pH, f(pH) functions, described below. We

195 represented the temperature effect, f(T), using a classic Q_{10} function:

196 $$f(T) = Q_{10_i}^{\frac{\text{Temperature}_{\text{soil}} - \text{Temperature}_{\text{reference}}}{10}} \tag{5}$$

197 We represented the pH effect, f(pH), based on Cao et al. (1995):

198 $$f(pH) = \frac{(pH - pH_{\text{minimum}})*(pH - pH_{\text{maximum}})}{(pH - pH_{\text{minimum}})*(pH - pH_{\text{maximum}})-(pH - pH_{\text{optimum}})^2} \tag{6}$$

199 where we set the minimum, optimum, and maximum soil pH values to 4, 7, and 10, respectively. Following Xu et al.

200 (2015), we considered the contribution of acetate to pH as follows:

201 $$pH = -1 * \log(10^{pH_{\text{initial}}} + 4.2E - 9 * \text{Acetate}) \tag{7}$$

202 Although other mechanisms to alter soil pH are present at the site, e.g., Fe reduction and oxidation (Teh et al., 2005;

203 Hall and Silver, 2013), these are not considered in the model at this time. Calibrated values of $\text{GrowR}_{\text{func}_i}$,

204 $\text{DeadR}_{\text{func}_i}$, $\text{Efficiency}_{\text{func}_i}$, $\text{KM}_{\text{func}_i}$, and Q_{10_i} are presented in Table 1.

205 **2.4.2 Diffusion module for gaseous and solute transport in soil profile and across soil-air boundary**

206 In order to account for the diffusion of gases across the soil-air boundary and solutes (e.g. acetate) through soil water

207 films (Fig. 1), we added the diffusion module of the Dual Arrhenius and Michaelis Menten (DAMM) model

208 (Davidson et al., 2012; Sihi, 2020; Sihi et al., 2018, 2020a) to the existing microbial functional group model, which

209 we refer to as M3D-DAMM. We calculated initial concentration of gases like O$_2$, H$_2$, CO$_2$, and CH$_4$, [Gas$_{\text{conc}}$], (unit:

210 V V^{-1}), as a function of a unitless diffusion coefficient of gas in air (D$_{gas}$), volume fraction of gas in air (V V^{-1}), and

211 gas diffusivity (a$^{4/3}$) as follows:

212 $[Gas_{conc}] = D_{gas} \times$ atmospheric concentration $\times a^{4/3}$ (8)

213 where a$^{4/3}$ represents the tortuosity of diffusion pathway for gases as a function of soil water (SoilM) and

214 temperature (SoilT):

215 $a^{4/3} = \left(Porosity - \frac{SoilM}{100} \right)^{4/3} \times \left(\frac{SoilT+273.15}{293.15} \right)^{1.75}$ (9)

216 where the air-filled porosity (a) was calculated by subtracting the volume fraction of soil moisture (V V^{-1}) from total

217 porosity. Porosity was calculated as:

218 $(1 - \frac{Bulk\ density}{Particle\ density})$ (10)

219 The exponent of 4/3 accounts for diffusivity of gases through porous media (Davidson and Trumbore, 1995). The

220 exponent of 1.75 represents the temperature response of gaseous diffusion (Massman, 1998; Davidson et al., 2006).

221 Following Davidson et al. (2012), the value used for gaseous diffusivity coefficient (D$_{gas}$) was calculated based on

222 an assumed boundary condition such that the concentration of gaseous substrates in the soil pore space would be

223 equivalent to the volume fraction of gases in air under completely dry conditions.

224 We assumed another boundary condition to determine the value of the aqueous diffusion coefficient, D$_{liq}$, such that

225 soluble substrates like acetate would be available at the enzymatic reaction site under conditions with saturating soil

226 water content (Davidson et al., 2012):

227 $D_{liq} = \frac{1}{Porosity^3}$ (11)

228 We represented soluble substrates (acetate) diffused through a soil water film as $Aqueous - substrate$ (µM L^{-1}),

229 which we calculated as follows:

230 $Aqueous - substrate_{av} = Aqueous - substrate \times D_{liq} \times (\frac{SoilM}{100})^3$ (12)

231 where the $(\frac{SoilM}{100})^3$ term represents the diffusion rate of aqueous substrates to the enzymatic active site (Papendick

232 and Campbell, 1981). Concentrations of acetate in the aqueous phase (µM L^{-1}) were obtained from the

233 measurements across the catena averaged by depths (10 and 30 cm) of rhizon samplers.

234 We calculated CH$_4$ emissions, $CH_{4emission}$ (unit: µmole m^{-2} hr^{-1}), as a function of concentration ($[CH_{4conc}]$),

235 production (CH_{4prod}), and oxidation (CH_{4ox}) of CH$_4$, multiplied by the equivalent "depth" (set to 15 cm) (for cm^{-3}

236 volume to cm^{-2} area conversion) and 10^4 (for m^2 to cm^2 conversion) as follows:

237 $CH_{4emission} = [CH_{4conc}] + (CH_{4prod} - CH_{4ox}) \times 10^4 \times depth$ (13)

238 **2.4.3 Soil microsites**

239 The importance of diverse microsite conditions was inferred based on many previous observations in the field and

240 the lab of co-occurrences of oxic soil concentrations and reduced redox-active species (Silver et al., 1999; Teh et al.,

241 2005; Megonigal and Geunther 2008; Hall et al. 2013, 2016; Sihi et al., 2020a). The high clay content, abundant Fe

242 oxides, and visible redox mottling, particularly in the valley and slope soils facilitates a diversity of soil micro-

243   environments where O_2 and CH_4 can seemingly co-occur, albeit in different microsite locations (Silver et al., 1999;

244   Teh and Silver, 2006). Microsite diversity was also invoked to help explain the rapid CH_4 emissions following

245   drought at the field site (O'Connell et al., 2018). Techniques for accurately measuring in-situ microsite activities

246   remain very limited to date, here or elsewhere. Therefore, we simulated production, consumption, and diffusion

247   processes within soil microsites using a log-normal probability distribution function of soil moisture and available C

248   based on these previously observed relationships (Fig. 1). The average values of individual processes across

249   simulated microsites (represented by "i") represent the reaction in the bulk soil, which we constrained using the net

250   measured CH_4 emissions.

251     $$\text{Bulk soil}_{average} = \frac{\sum \text{Frequency}_i \times [\text{microsite}]_i}{\text{Total microsites}} \qquad (14)$$

252   We directly adopted the probability distribution function of soil moisture and C from Sihi et al. (2020a), which

253   constrained values of Frequency_i of soil microsites. We a priori assigned the size of the microsites to be at least an

254   order magnitude smaller than the diameter used for bulk measurements of CH_4 fluxes. Thus, the mean diameter of

255   microsites was assumed to be at the mm-scale (the size-class of small stable aggregates in these soils), as the

256   diameter of soil chambers was 15.24 cm. Thus, the resultant number of total microsites below each soil flux

257   chamber was 10,000.

258   **2.4.4 Sensitivity Analysis**

259   We evaluated the sensitivity of model parameters with a global variance-based sensitivity analysis using the *R-*

260   *multisensi* package. This method uses a global sensitivity index ($0 < GSI < 1$) to determine the sensitivity of CH_4

261   emissions to model parameter values (Bidot et al., 2018). We conducted a multivariate technique to estimate GSI

262   values in sequential steps. First, we implemented a factorial design on the uncertain model parameters, which is

263   followed by a principal component analysis on model outputs. Then, we extracted GSI values by an ANOVA-based

264   sensitivity analysis on the first principal component. To that end, parameters with high GSI values may explain high

265   temporal variations of the observed CH_4 emissions and those with low GSI values are insignificant to reproduce the

266   temporal dynamics of CH_4 emissions.

267   **2.4.5 Statistical Analysis**

268   We used R (version 3.5.1) for statistical analyses, modeling, and visualization purposes (R Core Team, 2018).

269   Statistical analyses and figures were produced using *R-ggstatsplot* (Patil, 2018) and *R-ggplot2* (Wickham, 2016)

270   packages. Differences in soil and porewater chemistry across the catena were compared using robust t-test.

271   Correlograms for soil temperature, soil moisture, O_2, and soil CH_4 emissions were created using adjusted Holm

272   correlation coefficients. All statistical analyses were conducted at the 5% significance level. We implemented the

273   M3D-DAMM model using *R-FME* package (Soetaert, 2016).

3 Results

3.1 Observational dynamics of soil biogeochemistry

Soil and porewater chemistry varied along the catena (Fig. 2). Dissolved organic carbon (DOC) values followed the trend of ridge > slope > valley (p ≤ 0.001). Soil DOC concentrations (mean ± SE) were 0.55 ± 0.10, 0.30 ± 0.03, and 0.18 ± 0.03 mg g^{-1} in ridge, slope, and valley soils, respectively. Organic acid (acetate) concentrations were significantly higher in the ridge (6.57 ± 1.48 µM L^{-1}) and slope (6.42 ± 2.19 µM L^{-1}) than in the valley (1.80 ± 0.20 µM L^{-1}) (p = 0.003). Soil pH followed the trend of valley > slope > ridge (p < 0.001). Average soil pH ranged from 4.25 ± 0.11 in the ridge, to 4.49 ± 0.08 in the slope, and to 5.05 ± 0.09 in the valley.

Soil moisture and soil O_2 concentrations were distinctly different in the drought year (2015) compared to 2016. The drought in 2015 decreased soil moisture in the slope and ridge soils and increased O_2 concentrations in the valley soils (Fig. 3) (also see O'Connell et al., 2018). Generally, average soil moisture was higher in the valley (0.47 ± 0.05 in 2015 and 0.51 ± 0.01 v v^{-1} in 2016) as compared to the ridge (0.31 ± 0.12 in 2015 and 0.39 ± 0.03 v v^{-1} in 2016) and slope (0.30 ± 0.16 in 2015 and 0.41 ± 0.04 v v^{-1} in 2016). Average O_2 concentrations were generally lower in the valley (11.54 ± 5.94 in 2015 and 6.30 ± 2.96 % in 2016) as compared to the ridge (18.37 ± 0.72 in 2015 and 17.52 ± 0.42 % in 2016) and slope (18.09 ± 1.22 in 2015 and 16.89 ± 0.58 % in 2016). After the drought ended, the recovery of soil moisture in the ridge and slope soils proceeded more quickly than the recovery of O_2 concentrations in the valley soils (Fig. 3). Soil temperature ranges were averaged across the topographic gradient and were similar in both years (average was 21.58 ± 1.88 in 2015 and 22.97 ± 1.04 °C in 2016).

In 2016, net CH_4 emissions were generally positive in the valley and were marginally negative in the ridge and slope (Fig. 4). The dynamics of CH_4 were very different following the 2015 drought, resulting in net positive CH_4 emissions in the post-drought period for all topographic positions (Fig. 3) (as described in more detail in O'Connell et al. 2018). The magnitude of CH_4 emissions was greater in the valley, followed by the slope and then the ridge. The strength of the relationships between net CH_4 emissions and soil temperature, moisture, and O_2 concentrations were contingent on both topographic position and year (2015 vs 2016) (Fig. 5). For example, the relation between CH_4 emissions and soil moisture was stronger in 2016 (normal year) than in 2015 (drought year). The correlation between CH_4 emissions and O_2 concentrations was stronger and more negative in 2015 than 2016. Correlations between soil moisture and O_2 concentrations were negative and stronger in 2016 than in 2015. Correlation coefficients between soil O_2 concentrations and CH_4 emissions were negative and strongest for valley soils and lowest for ridge soils in 2015, but were uncorrelated in 2016 for ridge and slope soils (Fig. S2).

3.2 Model simulations of methanogenesis and methanotrophy

In general, there was little bias in the relationships between the observed and simulated CH_4 emissions (Fig. 6). The model explained 72% and 67% of the variation in soil CH_4 emissions for 2015 and 2016, respectively, although the model performance varied across the catena (Figs. 6, S3, S4). Overall, simulated CH_4 emissions captured the trend of valley > slope ≥ ridge for 2016. The model also captured the dramatically different dynamics of field CH_4

308   emissions as a function of topography during and after the 2015 drought. Net positive CH_4 emissions were simulated
309   in the drought recovery and post-drought periods in the ridge and slope in 2015, while net negative emissions were
310   simulated in the other times for these landscape positions. Additionally, simulated net CH_4 emissions were
311   decreased during the drought and drought recovery in the valley soils, as well as the strong net CH_4 emissions in the
312   valley soils in the post-drought period.
313   The ridge and slope positions were more similar to each other than to the valley soils. Simulated decreased
314   production of acetate and hydrogen during the 2015 drought in the ridge and slope positions resulted in decreased
315   biomass of aceticlastic methanogens and hydrogenotrophic methanogens (Figs. S5, S6). Gross CH_4 production
316   therefore decreased during these time periods (Fig. S7). Simultaneously, as soil moisture decreased, simulated
317   methanotrophic biomass increased during the drought (Fig. S5). The simulated biomass of both aceticlastic
318   methanogens and hydrogenotrophic methanogens increased dramatically in the ridge and slope soils during drought
319   recovery (aceticlastic methanogens: 3.3 and 5.3 times higher than drought period for ridge and slope, respectively;
320   hydrogenotrophic methanogens: 6.1 and 12 times higher than drought period for ridge and slope, respectively) and
321   post-drought (aceticlastic methanogens: 5.2 and 8.8 times higher than drought period for ridge and slope,
322   respectively; hydrogenotrophic methanogens: 12 and 24 times higher than drought period for ridge and slope,
323   respectively) period. Concomitantly, production of acetate and H_2 was much higher in the ridge and slope soils
324   during the drought recovery (acetate: 1.8 and 2.4 times higher than the drought period for ridge and slope soils,
325   respectively; H_2: 3.5 and 6.0 times higher than the drought period for ridge and slope soils, respectively) and the
326   post-drought (acetate: 2.3 and 3.2 times higher than the drought period for ridge and slope, respectively; H_2: 5.6 and
327   10 times higher than the drought period for ridge and slope, respectively) period. Together, gross CH_4 production in
328   the ridge and slope soils was significantly higher during the drought recovery (1.9 and 2.5 times higher than the
329   drought period for ridge and slope, respectively) and post-drought periods (3.4 and 4.6 times higher than the drought
330   period for ridge and slope, respectively) compared to the drought (Fig. S7). Simulated production of acetate was
331   increased that also lowered soil pH values during drought recovery (Fig. S6), with a more pronounced effect in the
332   ridge and slope soils. Additionally, simulated methanotrophic biomass and CH_4 oxidation decreased during the post-
333   drought period (Figs. S5, S7), which is the same time period during which net CH_4 production increased strongly.
334   For the valley soils, simulated values of aceticlastic methanogens and concomitant acetate production increased
335   during the 2015 drought (Figs. S5, S6). During the drought recovery and post-drought period, both aceticlastic
336   methanogens and acetate production decreased in the valley, while hydrogenotrophic methanogens and H_2
337   production were stable. Gross CH_4 production, however, remained relatively flat during the drought event in the
338   valley, and only increased during the post-drought period (Fig. S7). Simulated CH_4 oxidation and methanotrophic
339   biomass, on the other hand, increased dramatically during the drought and drought recovery period (Figs. S5, S7),
340   and then decreased strongly during the post-drought period. However, simulated methanotrophic biomass was
341   smaller in the valley soils compared to the ridge and slope soils. Methane oxidation by methanotrophs exerted strong
342   controls on simulated net CH_4 emissions, not only in the valley but in all the topographic positions.

3.3 The influence of microsites on net methane emissions

Concomitant with decreased soil moisture, the simulated diffusion of gases (O_2, H_2) was enhanced during the drought event in 2015, while diffusion of the solute (acetate) was dramatically decreased, particularly for the ridge and slope soils (Fig. S8). However, reduction in soil moisture and increase in O_2 can inhibit fermentative hydrogen production (Cabrol et al., 2017). Consequently, simulated gross CH_4 production through hydrogenotrophic and aceticlastic pathways both decreased during the drought event for the ridge and slope positions (Figs. S7, S9). As soil moisture increased during the drought recovery and post-drought periods, the diffusion of gases decreased, and diffusion of acetate increased in the ridge and slope soils (Fig. S8). Consequently, simulated values of gross CH_4 production increased and gross CH_4 oxidation decreased during drought recovery and the post-drought period (Fig. S7). These factors likely contribute to the large pulses of net CH_4 emissions during the post-drought period for ridge and slope positions (Fig. 3).

Overall, the valley soils were relatively insensitive to changes in the diffusion rate of either gases or solutes (Fig. S8), most likely because soil moisture remained relatively stable, regardless of drought conditions (Fig. 3). The lower sand and higher clay contents in the valley soils (Brenner et al., 2019), as well as the lower topographic position, likely caused the valley soils to remain wetter than the slope and ridge soils. Therefore, simulated values of gross CH_4 production were fairly stable in the valley soils (Fig. S7) during the drought and drought recovery period. Simulated production, oxidation, and net flux of CH_4 was further modified by reactions occurring within soil microsites. For example, during the drought (~DOY 200 in 2015), gross CH_4 production was more frequent in soil microsites in the valley compared to the slope and ridge (Fig. 7). Simulated values of CH_4 oxidation were much greater in microsites in the slope and ridge positions, so the net CH_4 emissions were positive in the valley soils and negative in the ridge and slope positions. During the 2015 post-drought period (DOY 345), the frequency of CH_4 production was much greater in all topographic positions compared to the drought period (DOY 200), and it was also more enhanced in the valley soils compared to the slope and ridge. Thus, net positive CH_4 emissions were observed in all topographic positions in the post-drought period (Fig. 3). Methane oxidation at DOY 345 was much greater in the ridge and slope compared to the valley, similar to predictions at DOY 200. Therefore, the prominent CH_4 emissions from all three topographic positions were primarily due to increased production (CH_4 production on DOY 345 was 150, 248, and 80 % higher than DOY 200 in ridge, slope, and valley, respectively) rather than decreased oxidation (CH_4 oxidation was 32, 31, and 43 % lower on DOY 345 than DOY 200 in ridge, slope, and valley, respectively), which agrees with previous studies in our site (Teh et al., 2005, 2008; von Fischer and Hedin, 2002).

Diffusion into microsites strongly affected the concentrations of gases and solutes experienced by microbes, and differences as a function of topographic position were again predicted. Acetate production and diffusion were enhanced in valley soils during the drought, when compared to the slope and ridge soils (Fig. S10). The H_2 production was also enhanced in the valley soils during the drought, but the wetter valley soils experienced lower rates of H_2 diffusion compared to the ridge and slope soils. Increases in O_2 diffusion were also apparent in the ridge and slope soils during the drought, and those increases were greater than in the valley soils. During the post-drought

379 period, however, the frequency of H_2 and O_2 diffusion was much greater for the ridge soils compared to the valley

380 soils (Fig. S10).

381 Of all parameters, the most sensitive ones were those that controlled CH_4 production through the aceticlastic

382 pathway, followed by the parameters related to CH_4 oxidation (Fig. 8). The GSI values for parameters related to

383 aceticlastic methanogenesis and methanotrophy ranged between 0.25 - 0.75, whereas the corresponding GSI values

384 for hydrogenotrophic methanogenesis were always < 0.1.

385 **4 Discussion**

386 **4.1 Mechanisms governing net methane emissions**

387 Although the initial concentrations of available C for fermentation (i.e. DOC) and substrate for aceticlastic

388 methanogenesis (i.e. acetate) in the bulk soil followed the trend of ridge > slope > valley (Fig. 2), the pattern of net

389 CH_4 emissions across the catena was opposite (valley > slope $\geq$ ridge), especially in 2016 (Fig. 4). The seemingly

390 counterintuitive relations of substrate concentrations in the bulk soil versus net CH_4 emissions can be explained by

391 modeling the differing redox conditions across soil microsites. Diffusion promoted the availability of the acetate

392 substrate through more connected soil water films in the wetter valley soils and caused higher gross CH_4 production

393 in 2016, as compared to the relatively drier slope and ridge soils (Figs. S7, S8). In contrast, diffusion of gaseous

394 methanotrophic substrates (CH_4 and O_2) was promoted in the air-filled pore spaces in the drier ridge and slope soils

395 (Fig. S8), resulting in reduced net CH_4 emissions for these two topographic positions in 2016 (Fig. 4). Further,

396 reduced diffusion of O_2 in the wetter valley soils decreased gross methanotrophy compared to the slope and ridge

397 soils (Figs. S7, S8). Consequently, in 2016, net CH_4 emissions dominated the valley soils but were minimal in the

398 ridge and slope soils.

399 On the other hand, the drought event in 2015 decreased the simulated CH_4 emission in the slope and ridge soils by

400 decreasing H_2 production, and both production (Fig. S6) and diffusion of acetate (Fig. S8). The drought increased

401 the CH_4 sink strength of both ridge and slope soils as the observed net CH_4 emissions became more negative during

402 the drought compared to the pre-drought period (Fig. 3). Contributing factors predicted by the model include

403 enhanced O_2 diffusion into the drier ridge and valley soils (Fig. S8), as well as enhanced methanotrophic biomass

404 (Fig. S5). In the valley, the primary impact of the drought appeared to be due to increased methanotrophy (Fig. S7),

405 since acetate, H_2, and gross CH_4 production were predicted to continue unabated (Fig. S6, S7). This suggests that

406 drought enhanced consumption of atmospheric CH_4 in our site, which is consistent with findings from natural

407 droughts and throughfall exclusion experiments in other wet tropical forest soils (Aronson et al., 2019; Davidson et

408 al., 2004, 2008; Wood and Silver, 2012).

409 However, simulation of observed CH_4 emission during drought recovery in 2015 required explicit representations of

410 the complex interaction of the diffusive supply of solute and gases, dynamics of the microbial functional groups, and

411 the associated acetate-pH feedback loop across the distribution of soil microsites (Fig. 3). The drought recovery

412 increased soil moisture which likely prompted anaerobiosis across all topographic locations by significantly

413 reducing gas diffusivity in a fraction of the simulated microsites (11, 17, and 21 % in ridge, slope, and valley,

414   respectively) (McNicol and Silver, 2014; Sihi et al., 2020a; Teh et al., 2005). The return to dominantly reducing

415   conditions also was predicted to stimulate fermentation and the production of acetate through homoacetogenesis

416   (Fig. S6). Enhanced production and diffusion of acetate during recovery (Fig. S8) triggered growth in the predicted

417   biomass of aceticlastic methanogens (Fig. S5), which in turn, increased rates of aceticlastic methanogenesis (Fig.

418   S9).

419   Simulated rates of hydrogenotrophic methanogenesis also increased in anaerobic microsites (Figs. S9, S10),

420   mediated by increased production of H_2 and subsequent stimulation of the biomass of hydrogenotrophic

421   methanogens during the drought recovery in 2015 (Fig. S5). Overall, the absolute values of simulated gross CH_4

422   production through hydrogenotrophic and aceticlastic pathways (Fig. S9) outweighed the simulated gross CH_4

423   oxidation rates (Fig. S7), resulting in net soil CH_4 emissions across the catena during the post-drought period (Fig.

424   3).

425   Acetate-driven CH_4 increases, decreases in methanotrophy due to decreasing O_2, and increasing hydrogenotrophic

426   methanogenesis all contributed to the post-drought pulses of CH_4 (Fig. 8). Both kinds of methanogens increase

427   during drought recovery and post-drought, but aceticlastic methanogens were two orders of magnitude more

428   abundant than hydrogenotrophic methanogens. Additionally, acetate may accumulate in microsites during drought,

429   and then become more available with drought recovery due to enhanced solute diffusion (Fig. S8). The model

430   simulations suggest that hydrogen diffusion was lessened under the drought recovery which is consistent with

431   decreasing rates of gas diffusion through saturated soils (Fig. S8). Further, H_2 has a faster turnover rate compared to

432   acetate (Xu et al. 2015) and therefore accumulation in soils, especially shallow soils which are the subject of this

433   study, is minimized. So, acetate versus hydrogen substrate availability in microsites better explains the observations

434   of higher CH_4 production under the post-drought conditions.

435   Additionally, acetate is a source of proton and should reduce soil pH (Amaral et al., 1998; Conrad and Klose, 1999;

436   Jones et al., 2003). Previous studies (Xu et al., 2015; Xu et al., 2010) demonstrated that acetate-driven soil pH

437   reduction can reduce net CH_4 production by as much as 30%, especially in systems with low initial soil pH like our

438   study site. Given that optimal pH for biological activities peaks near neutral pH, the relatively higher soil pH in the

439   valley versus ridge and slope soil further enhanced the topographic patterns of CH_4 emissions (Conrad, 1996; also

440   see Figs. 2, 3, and 4). Note that the initial soil pH across the landscape was already in the acidic range (Fig. 2),

441   consequently, the simulated acetate production and concomitant decrease in soil pH during the 2015 drought

442   recovery further suppressed gross CH_4 production in ridge soils in comparison to the valley soils (Figs. S6 and S7).

443   Iron reducing bacteria can also suppress CH_4 production either by competing with aceticlastic methanogens for

444   acetate substrate or controlling the flow of acetate to both hydrogenotrophic and aceticlastic methanogens by

445   dissimilatory iron reduction (Teh et al., 2008). Additionally, Fe reduction can increase soil pH either by proton

446   consumption and colloid dispersion, while Fe oxidation can lead to more acidic conditions (Hall and Silver, 2013;

447   Thompson et al., 2006). None of the Fe-associated mechanisms are currently represented in the M3D-DAMM

448   model.

449   Hence, high temporal resolution field-scale measurements of CH_4 emissions and soil and porewater chemistry

450   facilitated evaluation of the combined effects of soil redox conditions (moisture and O_2 concentrations) and

451 associated pH feedbacks on underlying processes occurring across soil microsites, while accounting for variation

452 along the catena as a result of changing climatic drivers over time. The M3D-DAMM model captured the Birch-type

453 effect by quantifying the pulses in soil CH_4 emissions as a function of increases in soil moisture following a strong

454 drought (Birch, 1958). Specifically, the model coupled with microsite diffusivity explained CH_4 emissions common

455 to wet valley soils and rare in comparatively drier ridge and slope soils and predicted the net release of CH_4

456 emissions from all topographic positions following a strong drought.

457 **4.2 Sensitivity analysis**

458 The variance-based sensitivity analysis confirmed the importance of microbial functional groups and their complex

459 interactions with the surrounding biophysical and chemical environments in controlling CH_4 production and

460 oxidation. For example, the growth and death of aceticlastic methanogens and the relative efficiency of aceticlastic

461 methanogenesis were the most sensitive parameters (Fig. 8), which is consistent with another modeling effort on

462 CH_4 fluxes across the Arctic landscape (Wang et al., 2019). Although from completely different ecosystem types,

463 Wang et al. (2019) and the present study confirmed the importance of simulating soil topographies and microbial

464 mechanisms when evaluating the heterogeneities in CH_4 fluxes. Representations of both direct (methanogenic

465 substrate) and indirect (soil pH feedback) effects of acetate may have contributed to higher GSI values for

466 parameters representing aceticlastic methanogenesis, which is similar to a previous study (Xu et al., 2015). The

467 sensitivity of CH_4 emissions to the parameters representing methanotrophy were secondary to those representing

468 aceticlastic methanogenesis, which is consistent with the increase in methanotrophic biomass during the drought.

469 Our predicted changes in microbial biomass might be unacceptably large for the entire soil microbial community,

470 which may only double or perhaps quadruple in response to changes in conditions, but individuals can grow

471 exponentially (Goberna et al. 2010; Pavlov and Ehrenberg 2013; Roussel et al. 2015; Buan 2018).

472 **4.3 Other processes**

473 We did not completely reproduce the net emissions of soil CH_4 during the 2015 post-drought period across the

474 catena with the M3D-DAMM model. To capture the full potential of net emissions of CH_4 (white shading in Fig. 3)

475 from sesquioxide-rich soils, future modeling efforts may need to explicitly include the dynamics of redox-sensitive

476 elements such as Fe and associated pH feedback under contrasting redox conditions (Barcellos et al., 2018;

477 Bhattacharyya et al., 2018; Hall and Silver, 2013, 2015, 2016; O'Connell et al., 2018; Parfitt et al., 1975; and Silver

478 et al., 1999). Wetting events can lower soil redox potential and reduce electron acceptors like Fe(III) to Fe(II). This

479 concomitant reduction of Fe may increase soil pH, especially in anaerobic microsites, which could further increase

480 net emissions of soil CH_4 (Tang et al., 2016; Zheng et al., 2019). Accounting for these effects may allow model

481 simulations to better match the highest observed net CH_4 emissions in the post-drought period (Fig. 3).

482 Additionally, the reduction of Fe(III) to Fe(II) has supported anaerobic CH_4 oxidation in other ecosystems (Ettwig et

483 al., 2016). Within this context, a measurable amount of anaerobic oxidation of CH_4 has previously been reported at

484 our study site (Blazewicz et al., 2012). Additionally, Fe-reducing microorganisms can utilize acetate as a substrate

485 and thereby compete with methanogens and reduce net methane emissions (Teh et al., 2008). Given the gradient of

486   Fe in our study site, it is likely that biogeochemical cycling of Fe and CH_4 are coupled (O'Connell et al., 2018)

487   which should be accounted for in future modeling efforts. For example, a modeling study supported the importance

488   of Fe in simulating CH_4 cycling in an Arctic soil (Tang et al., 2016). To that end, building a comprehensive

489   framework that also includes Fe biogeochemistry will afford greater confidence in projected CH_4 emissions from

490   wet tropical forests under future climatic conditions (Bonan et al., 2008; Pachauri et al., 2014; Xu et al., 2016).

491   **5 Conclusions**

492   High-frequency CH_4 emission measurements coupled with real-time soil chemical measurements identified spatial

493   and temporal variations affecting CH_4 production and oxidation in wet tropical forest soils of Puerto Rico. Overall,

494   contrasting patterns of soil moisture between ridge and valley soils played an instrumental role in governing net CH_4

495   emissions. For example, consistently greater soil moisture likely favored methanogenesis by lowering the

496   availability of O_2 in valley soils compared to ridgetop soils, especially in microsites with high soil moisture and soil

497   C content. However, soil porewater chemistry, particularly the concentrations of acetate and associated soil pH

498   influenced the pattern of net emissions of CH_4 across the catena (valley > slope > ridge) during wetting after the

499   2015 drought. Thus, our results provide compelling evidence of the importance of both hot spots and hot moments

500   in generating and mediating CH_4 emissions in wet tropical forest soils. A microbial functional group-based model

501   coupled with a diffusivity module and consideration of soil microsites adequately reproduced both the spatial and

502   temporal dynamics of soil CH_4 emissions, although mechanisms involving Fe biogeochemistry were neglected.

503   This study suggests that representing the microbial mechanisms and the interactions of microbial functional groups

504   with the soil biophysical and chemical environment across soil microsites is critical for modeling CH_4 production

505   and consumption. To that end, explicit consideration of these underlying mechanisms improved predictions of CH_4

506   dynamics in response to regional climatic events and provided insig ht into differential dynamics of solute and gas

507   diffusion, different microbial functions, and gross CH_4 production and oxidation as a function of topography. Hence,

508   we contribute to the ongoing development and improvements of Earth system and process models to better simulate

509   microbial roles in CH_4 cycling at regional and global scales. However, observational data concerning the activities

510   of different soil microbial functional groups is still needed to confirm the mechanisms proposed here. Future studies

511   should integrate geochemical and microbiological information relevant for oscillatory redox conditions in wet

512   tropical forests, especially those related to the redox-sensitive elements to build a comprehensive framework for

513   modeling tropical soil CH_4 emissions.

514   **Code and data availability**

515   Meteorological data (http://criticalzone.org/luquillo/data/dataset/4723/) are available from the Luquillo CZO

516   repository. 2015 greenhouse gas fluxes (DOI: 10.6073/pasta/316b68dd254e353e1acfb16d92bac2dc) are available

517   from the Luquillo LTER repository. The 2016 greenhouse gas fluxes (DOI: 10.15485/1632882), soil chemistry

518   (DOI: 10.15485/1618870), and rhizon lysimeter data (DOI: 10.15485/1618869) are available from ESS-DIVE

519   repository. R scripts used for this modeling exercise are archived at the following Zenodo repository (DOI:

520   10.5281/zenodo.3890562).

Author contributions

DS performed the data curation of 2016 flux data and the soil and lysimeter data, collated diffusion and microsite processes into the model presented herein, interpreted and validated the model application, developed the visualization, and wrote the original draft. XX provided the model code used in the investigation and assisted with its modification and application. MSO collected the 2016 field flux data. CSO and WLS provided the 2015 flux data and the 2015-2016 field soil measurements for temperature, oxygen, and moisture. CSO developed workflow for field flux data management, cleaning and analysis. WLS acquired the funding, administered the project, and supervised the research team involved with collection of the 2015 data. CLL collected the rhizon water samples and soil samples from the field site, with assistance from MAM. JMB analyzed the rhizon water samples in the lab. JRP, RKQ, and JMB completed the laboratory soil analyses. BDN supplied, installed, and maintained the rhizon water samplers. MAM acquired the funding and administered the project that collected the 2016 data, conceptualized the paper and proposed the methods, supervised the research team, and contributed to the writing, interpretation, and visualization of subsequent drafts. All authors contributed to the manuscript through reviewing and editing subsequent drafts.

Competing interests

The authors declare that they have no conflicts of interest.

Acknowledgements

We appreciate the site access and support facilitated by Dr. Grizelle González of the U.S. Department of Agriculture (USDA) Forest Service International Institute of Tropical Forestry and by Dr. Jess Zimmerman of the University of Puerto Rico at Rio Piedras (UPR). We thank Dr. William McDowell of the University of New Hampshire (UNH) for logistical support. We thank Mr. Brian Yudkin, Ms. Jordan Stark, and Ms. Gisela Gonzalez for assistance with field data and sample collection. This work was supported through an Early Career Award to MAM through the U.S. Department of Energy (DOE) Biological and Environmental Research Program; and by grants from the US DOE (TES-DE-FOA-0000749) and the National Science Foundation (NSF) (DEB-1457805) to WLS, as well as the NSF Luquillo Critical Zone Observatory (EAR-0722476) to UNH and the NSF Luquillo Long Term Ecological Research Program (DEB-0620910) to UPR. WLS received additional support from the USDA National Institute of Food and Agriculture, McIntire Stennis project CA-B-ECO-7673-MS. This research used resources of the Compute and Data Environment for Science (CADES) at the Oak Ridge National Laboratory, which is managed by UT-Battelle, LLC, under contract DE-AC05-00OR22725 with the U.S. Department of Energy.

References

Amaral, J. A., Ren, T., and Knowles, R.: Atmospheric methane consumption by forest soils and extracted bacteria at different pH values, Appl. Environ. Microbiol., 64, 2397-2402, 1998.

553 Andersen, B. L., Bidoglio, G., Leip, A., and Rembges, D.: A new method to study simultaneous methane oxidation
554 and methane production in soils, Global Biogeochem. Cy., 12, 587-594, https://doi.org/10.1029/98GB01975, 1998.
555 Aronson, E. L., Dierick, D., Botthoff, J., Oberbauer, S., Zelikova, T. J., Harmon, T. C., Rundel, P., Johnson, R. F.,
556 Swanson, A. C., and Pinto-Tomás, A. A.: ENSO-influenced drought drives methane flux dynamics in a tropical wet
557 forest soil, J. Geophys. Res.-Biogeo., 124, 2267-2276, https://doi.org/10.1029/2018JG004832, 2019.
558 Barcellos, D., O'Connell, C. S., Silver, W., Meile, C., and Thompson, A.: Hot spots and hot moments of soil
559 moisture explain fluctuations in iron and carbon cycling in a humid tropical forest soil, Soil Systems, 2, 59,
560 https://doi.org/10.3390/soilsystems2040059, 2018.
561 Bhattacharyya, A., Campbell, A. N., Tfaily, M. M., Lin, Y., Kukkadapu, R. K., Silver, W. L., Nico, P. S., and Pett-
562 Ridge, J.: Redox fluctuations control the coupled cycling of iron and carbon in tropical forest soils, Environ. Sci.
563 Technol., 52, 14129-14139, https://doi.org/10.1021/acs.est.8b03408, 2018.
564 Bidot, C., Monod, H., and Taupin, M.-L: A quick guide to multisensi, an R package for multivariate sensitivity
565 analyses, [Available at https://mran.microsoft.com/snapshot/2017-08-
566 06/web/packages/multisensi/vignettes/multisensi-vignette.pdf.], 2018.
567 Birch, H.: The effect of soil drying on humus decomposition and nitrogen availability, Plant Soil, 10, 9-31, 1958.
568 Blazewicz, S. J., Petersen, D. G., Waldrop, M. P., and Firestone, M. K.: Anaerobic oxidation of methane in tropical
569 and boreal soils: ecological significance in terrestrial methane cycling, J. Geophys. Res.-Biogeo., 117,
570 https://doi.org/10.1029/2011JG001864, 2012.
571 Bonan, G. B.: Forests and climate change: forcings, feedbacks, and the climate benefits of forests, Science, 320,
572 1444-1449, 10.1126/science.1155121, 2008.
573 Bosse, U., and Frenzel, P.: Methane emissions from rice microcosms: the balance of production, accumulation and
574 oxidation, Biogeochemistry, 41, 199-214, 1998.
575 Brenner, J., Porter, W., Phillips, J. R., Childs, J., Yang, X., and Mayes, M. A.: Phosphorus sorption on tropical soils
576 with relevance to Earth system model needs, Soil Res., 57, 17-27, https://doi.org/10.1071/SR18197, 2019.
577 Buan, N. R.: Methanogens: pushing the boundaries of biology: Emerging Topics in Life Science, 2, 629-646,
578 https://doi.org/10.1042/ETLS20180031, 2018.
579 Cabrol, L., Marone, A., Tapia-Venegas, E., Steyer, J. P., Ruiz-Filippi, G., and Trably, E.: Microbial ecology of
580 fermentative hydrogen producing bioprocesses: useful insights for driving the ecosystem function, FEMS microbiol.
581 Rev., 41, 158-181, https://doi.org/10.1093/femsre/fuw043, 2017.
582 Cabugao, K. G., Yaffar, D., Stenson, N., Childs, J., Phillips, J.; Mayes, M. A., Yang, X., Weston, D. J., and Norby,
583 R. J.: bringing function to structure: Root-soil interactions shaping phosphatase activity throughout a soil profile in
584 Puerto Rico, Ecol. Evol. (in press).
585 Cao, M., Dent, J., and Heal, O.: Modeling methane emissions from rice paddies, Global Biogeochem. Cy., 9, 183-
586 195, https://doi.org/10.1029/94GB03231, 1995.
587 Cattânio, J. H., Davidson, E. A., Nepstad, D. C., Verchot, L. V., and Ackerman, I. L.: Unexpected results of a pilot
588 throughfall exclusion experiment on soil emissions of CO_2, CH_4, N_2O, and NO in eastern Amazonia, Biol. Fert.
589 Soils, 36, 102-108, 10.1007/s00374-002-0517-x, 2002.
590 Chadwick, R., Good, P., Martin, G., and Rowell, D. P.: Large rainfall changes consistently projected over
591 substantial areas of tropical land, Nat. Clim. Change, 6, 177-181, 10.1038/NCLIMATE2805, 2016.
592 Conrad, R.: Soil microorganisms as controllers of atmospheric trace gases (H_2, CO, CH_4, OCS, N_2O, and NO),
593 Microbiol. Mol. Biol. Rev., 60, 609-640, 1996.
594 Conrad, R., and Klose, M.: Anaerobic conversion of carbon dioxide to methane, acetate and propionate on washed
595 rice roots, FEMS Microbiol. Ecol., 30, 147-155, https://doi.org/10.1111/j.1574-6941.1999.tb00643.x, 1999.
596 Cusack, D. F., Silver, W. L., and McDowell, W. H.: Biological nitrogen fixation in two tropical forests: ecosystem-
597 level patterns and effects of nitrogen fertilization, Ecosystems, 12, 1299-1315, 2009.
598 Davidson, E. A., Ishida, F. Y., and Nepstad, D. C.: Effects of an experimental drought on soil emissions of carbon
599 dioxide, methane, nitrous oxide, and nitric oxide in a moist tropical forest, Glob. Change Biol., 10, 718-730,
600 https://doi.org/10.1111/j.1365-2486.2004.00762.x, 2004.
601 Davidson, E. A., Nepstad, D. C., Ishida, F. Y., and Brando, P. M.: Effects of an experimental drought and recovery
602 on soil emissions of carbon dioxide, methane, nitrous oxide, and nitric oxide in a moist tropical forest, Glob. Change
603 Biol., 14, 2582-2590, https://doi.org/10.1111/j.1365-2486.2008.01694.x, 2008.
604 Davidson, E. A., Samanta, S., Caramori, S. S., and Savage, K.: The Dual Arrhenius and Michaelis–Menten kinetics
605 model for decomposition of soil organic matter at hourly to seasonal time scales, Glob. Change Biol., 18, 371-384,
606 https://doi.org/10.1111/j.1365-2486.2011.02546.x, 2012.
607 Davidson, E. A., Savage, K. E., Trumbore, S. E., and Borken, W.: Vertical partitioning of CO_2 production within a
608 temperate forest soil, Glob. Change Biol., 12, 944-956, https://doi.org/10.1111/j.1365-2486.2005.01142.x, 2006.

Davidson, E. A., and Trumbore, S. E.: Gas diffusivity and production of CO_2 in deep soils of the eastern Amazon, Tellus B: Chem. Phys. Meteorol., 47, 550-565, https://doi.org/10.3402/tellusb.v47i5.16071, 1995.

Ettwig, K. F., Zhu, B., Speth, D., Keltjens, J. T., Jetten, M. S., and Kartal, B.: Archaea catalyze iron-dependent anaerobic oxidation of methane, P. Natl. A. Sci., 113, 12792-12796, https://doi.org/10.1073/pnas.1609534113, 2016.

Goberna, M., Gadermaier, M., García, C., Wett, B., Insam, H.: Adaptation of methanogenic communities to the cofermentation of cattle excreta and olive mill wastes at 37 °C and 55 °C, Appl. Environ. Microb., 76, 19, 6564-6571, doi:10.1128/AEM.00961-10, 2010.

Hall, S. J., and Silver, W. L.: Iron oxidation stimulates organic matter decomposition in humid tropical forest soils, Glob. Change Biol., 19, 2804-2813, https://doi.org/10.1111/gcb.12229, 2013.

Hall, S. J., and Silver, W. L.: Reducing conditions, reactive metals, and their interactions can explain spatial patterns of surface soil carbon in a humid tropical forest, Biogeochemistry, 125, 149-165, doi:10.1007/s10533-015-0120-5, 2015.

Hall, S. J., Liptzin, D., Buss, H. L., DeAngelis, K., and Silver, W. L.: Drivers and patterns of iron redox cycling from surface to bedrock in a deep tropical forest soil: A new conceptual model, Biogeochemistry, 130(1-2), 177-190, 2016.

Harris, N. L., Lugo, A. E., Brown, S., and Heartsill-Scalley, T. (Eds.): Luquillo Experimental Forest: Research history and Opportunities, EFR-1, Washington, DC: U.S. Department of Agriculture, 152 p., 2012.

Heartsill-Scalley, T., Scatena, F. N., Estrada, C., McDowell, W., and Lugo, A. E.: Disturbance and long-term patterns of rainfall and throughfall nutrient fluxes in a subtropical wet forest in Puerto Rico, J Hydrol., 333, 472-485, https://doi.org/10.1016/j.jhydrol.2006.09.019, 2007.

Johnson, A. H., Xing, H. X., and Scatena, F. N.: Controls on soil carbon stocks in El Yunque National Forest, Puerto Rico: Soil Sci. Soc. Am. J., 79, 294-304, doi:10.2136/sssaj2014.05.0199, 2014.

Jones, D., Dennis, P., Owen, A., and Van Hees, P.: Organic acid behavior in soils–misconceptions and knowledge gaps, Plant Soil, 248, 31-41, 2003.

Keller, M., and Matson, P. A.: Biosphere-atmosphere exchange of trace gases in the tropics: Evaluating the effects of land use changes, in: Global Atmospheric-Biospheric Chemistry, Springer, 103-117, 10.1007/978-1-4615-2524-0, 1994.

Liptzin, D., Silver, W. L., and Detto, M.: Temporal dynamics in soil oxygen and greenhouse gases in two humid tropical forests, Ecosystems, 14, 171-182, 10.1007/s10021-010-9402-x, 2011.

Marshall, T.: Gas diffusion in porous media, Science, 130, 100-102, 10.1126/science.130.3367.100-a, 1959.

Massman, W.: A review of the molecular diffusivities of H_2O, CO_2, CH_4, CO, O_3, SO_2, NH_3, N_2O, NO, and NO_2 in air, O_2 and N_2 near STP, Atmos. Environ., 32, 1111-1127, https://doi.org/10.1016/S1352-2310(97)00391-9, 1998.

McNicol, G., and Silver, W. L.: Separate effects of flooding and anaerobiosis on soil greenhouse gas emissions and redox sensitive biogeochemistry, J. Geophys. Res.-Biogeo., 119, 557-566, https://doi.org/10.1002/2013JG002433, 2014.

Megonigal, J. P., and Geunther, A. B.: Methane emissions from upland forest soils and vegetation, Tree Physiol., 28, 491-498, 2008.

Neelin, J. D., Münnich, M., Su, H., Meyerson, J. E., and Holloway, C. E.: Tropical drying trends in global warming models and observations, P. Natl. A. Sci., 103, 6110-6115, https://doi.org/10.1073/pnas.0601798103, 2006.

Narrowe, A. B., Borton, M. A., Hoyt, D. W., Smith, G. J., Daly, R. A., Angle, J. C., Eder, E. K., Wong, A. R., Wolfe, R. A., Pappas, A., Bohrer, G., Miller, C. S., and Wrighton, K. A.: Uncovering the diversity and activity of methylotrophic methanogens in freshwater wetland soils, mSystems, 4(6), e00320-19, doi: 10.1128/mSystems.00320-19, 2019.

O'Connell, C. S., Ruan, L., and Silver, W. L.: Drought drives rapid shifts in tropical rainforest soil biogeochemistry and greenhouse gas emissions. Nat. Commun., 9, 1-9, 10.1038/s41467-018-03352-3, 2018.

Pachauri, R. K., Allen, M. R., Barros, V. R., Broome, J., Cramer, W., Christ, R., Church, J. A., Clarke, L., Dahe, Q., and Dasgupta, P.: Climate change 2014: Synthesis report. Contribution of Working Groups I, II and III to the Fifth Assessment Report of the Intergovernmental Panel on Climate Change, IPCC, 10013/epic.45156.d001, 2014.

Papendick, R., and Campbell, G. S.: Theory and measurement of water potential, Water Potential Relations in Soil Microbiology, 9, 1-22, https://doi.org/10.2136/sssaspecpub9.c1, 1981.

Parfitt, R. L., Atkinson, R. J., and Smart, R. S. C.: The mechanism of phosphate fixation by iron oxides, Soil Sci. Soc. Am. J., 39, 837-841, https://doi.org/10.2136/sssaj1975.03615995003900050017x, 1975.

Parton, W., Silver, W. L., Burke, I., Grassens, L., Harmon, M. E., Currie, W. S., King, J. Y., Adair, E. C., Brandt, L. A., Hart, S. C., and Fasth, B.: Global-scale similarities in nitrogen release patterns during long-term decomposition, Science, 315, 361-364, doi: 10.1126/science.1134853, 2007.

664   Patil, I.: ggstatsplot: "ggplot2" Based Plots with Statistical Details, [Available at https://CRAN.R-
665   project.org/package=ggstatsplot>], http://doi.org/10.5281/zenodo.2074621, 2018.
666   Pavlov, M. Y., and Ehrenberg, M.: Optimal control of gene expression for fast proteome adaptation to
667   environmental change, Proc. Natl. Acad. Sci. U.S.A., 110 (51), 20527-20532, doi/10.1073/pnas.1309356110, 2013.
668   Pumpanen, J., Kolari, P., Ilvesniemi, H., Minkkinen, K., Vesala, T., Niinistö, S., Lohila, A., Larmola, T., Morero,
669   M., and Pihlatie, M.: Comparison of different chamber techniques for measuring soil CO_2 efflux, Agr. Forest
670   Meteorol., 123, 159-176, https://doi.org/10.1016/j.agrformet.2003.12.001, 2004.
671   R Core Team.: R: A language and environment for statistical computing, Vienna, Austria, [Available at
672   https://www.r-project.org/], 2018.
673   Rochette, P., and Hutchinson, G. L.: Measurement of soil respiration in situ: Chamber techniques, Publications from
674   USDA-ARS / UNL Faculty, 1379, https://digitalcommons.unl.edu/usdaarsfacpub/1379, 2005.
675   Roussel E. G., Cragg, B. A., Webster, G., Sass, H., Tang, X., Williams, A. S., Gorra, R., Weightman, A. J., and
676   Parkes, R. J.: Complex coupled metabolic and prokaryotic community responses to increasing temperatures in
677   anaerobic marine sediments: Critical temperatures and substrate changes, FEMS Microbiology Ecology, 91, 2015,
678   fiv084, doi: 10.1093/femsec/fiv084, 2015.
679   Scatena, F. N.: An introduction to the physiography and history of the Bisley Experimental Watersheds in the
680   Luquillo Mountains of Puerto Rico, Gen. Tech. Rep. SO-72. New Orleans, LA: US Dept of Agriculture, Forest
681   Service, Southern Forest Experiment Station. 22 p., 72, 1989.
682   Scatena, F., and Lugo, A. E.: Geomorphology, disturbance, and the soil and vegetation of two subtropical wet
683   steepland watersheds of Puerto Rico, Geomorphology, 13, 199-213, https://doi.org/10.1016/0169-555X(95)00021-
684   V, 1995.
685   Sihi, D.: PR-model v1.0., 10.5281/zenodo.3890562, [available at
686   https://zenodo.org/record/3890562#.XuOP3DpKg2w], 2020.
687   Sihi, D., Davidson, E. A., Chen, M., Savage, K. E., Richardson, A. D., Keenan, T. F., and Hollinger, D. Y.: Merging
688   a mechanistic enzymatic model of soil heterotrophic respiration into an ecosystem model in two AmeriFlux sites of
689   northeastern USA, Agr. Forest Meteorol., 252, 155-166, https://doi.org/10.1016/j.agrformet.2018.01.026, 2018.
690   Sihi, D., Davidson, E. A., Savage, K. E., and Liang, D.: Simultaneous numerical representation of soil microsite
691   production and consumption of carbon dioxide, methane, and nitrous oxide using probability distribution functions,
692   Glob. Change Biol., 26, 200-218, https://doi.org/10.1111/gcb.14855, 2020a.
693   Sihi, D., López-Lloreda, C., Brenner J. M., Quinn R. K., Phillips J. R., Mayes, M. A.: Soil chemistry data across a
694   catena in the Luquillo Experimental Forest, Puerto Rico: A Comprehensive Framework for Modeling Emissions
695   from Tropical Soils and Wetlands, doi:10.15485/1618870, 2020b.
696   Sihi, D., López-Lloreda, C. Brenner J. M., Quinn R. K., Phillips J. R., Newman B. D., Mayes, M. A.: Porewater data
697   across a catena in the Luquillo Experimental Forest, Puerto Rico: A Comprehensive Framework for Modeling
698   Emissions from Tropical Soils and Wetlands, doi:10.15485/1618869, 2020c.
699   Sihi, D., Salazar-Ortiz, M., Mayes, M. A.: Soil chamber fluxes (CO2 and CH4) across a catena in the Luquillo
700   Experimental Forest, Puerto Rico: A Comprehensive Framework for Modeling Emissions from Tropical Soils and
701   Wetlands, doi:10.15485/1632882, 2020d.
702   Silver, W. L., Liptzin, D., and Almaraz, M.: Soil redox dynamics and biogeochemistry along a tropical elevation
703   gradient, in: Ecological gradient analyses in a tropical landscape, edited by: González, G., Willig, M. R., and Waide,
704   R. B., Ecol. Bull., Wiley-Blackwell, Hoboken, NJ, 54, 195-210, 2013.
705   Silver, W. L., Lugo, A., and Keller, M.: Soil oxygen availability and biogeochemistry along rainfall and topographic
706   gradients in upland wet tropical forest soils, Biogeochemistry, 44, 301-328, 1999.
707   Six, J., Bossuyt, H., Dergryze, S., Denef, K.: A history of research on the link between (micro)aggregates, soil biota,
708   and soil organic matter dynamics, Soil and Tillage Res., 79, 7–31, 2005.
709   Soetaert, K.: R Package FME: Inverse modelling, sensitivity, Monte Carlo—Applied to a dynamic simulation
710   model, (CRAN Vignette 2). [Available at https://cran. r-project. org/web/packages/FME/vignettes/FMEdyna. pdf.],
711   2016.
712   Soil Survey Staff: Order 1 Soil Survey of the Luquillo Long-Term Ecological Research Grid, Puerto Rico, USDA,
713   NRCS, https://luq.lter.network/content/order-i-soil-survey-luquillo-long-term-ecological-research-grid-puerto-rico,
714   1995.
715   Tang, G., Zheng, J., Xu, X., Yang, Z., Graham, D. E., Gu, B., Painter, S. L., and Thornton, P. E.: Biogeochemical
716   modeling of CO2 and CH4 production in anoxic Arctic soil microcosms, Biogeosciences, 13, 5021,
717   https://doi.org/10.5194/bg-13-5021-2016, 2016.

718 Teh, Y. A., Dubinsky, E. A., Silver, W. L., and Carlson, C. M.: Suppression of methanogenesis by dissimilatory Fe
719 (III)-reducing bacteria in tropical rain forest soils: Implications for ecosystem methane flux, Glob. Change Biol., 14,
720 413-422, https://doi.org/10.1111/j.1365-2486.2007.01487.x, 2008.
721 Teh, Y. A., and Silver, W. L.: Effects of soil structure destruction on methane production and carbon partitioning
722 between methanogenic pathways in tropical rain forest soils, J. Geophys. Res.-Biogeo., 111,
723 https://doi.org/10.1029/2005JG000020, 2006.
724 Teh, Y. A., Silver, W. L., and Conrad, M. E.: Oxygen effects on methane production and oxidation in humid tropical
725 forest soils, Glob. Change Biol., 11, 1283-1297, https://doi.org/10.1111/j.1365-2486.2005.00983.x, 2005.
726 Thomas, G. W.: Soil pH and soil acidity, Methods of Soil Analysis: Part 3 Chemical Methods, 5, 475-490,
727 https://doi.org/10.2136/sssabookser5.3.c16, 1996.
728 Thompson, A., Chadwick, O. A., Boman, S., and Chorover, J.: Colloid mobilization during soil iron redox
729 oscillations, Environ. Sci. Technol., 40, 5743-5749, https://doi.org/10.1021/es061203b, 2006.
730 Verchot, L. V., Davidson, E. A., Cattânio, J. H., and Ackerman, I. L.: Land-use change and biogeochemical controls
731 of methane fluxes in soils of eastern Amazonia, Ecosystems, 3, 41-56, https://doi.org/10.1007/s100210000009,
732 2000.
733 von Fischer, J. C., and Hedin, L. O.: Separating methane production and consumption with a field-based isotope
734 pool dilution technique, Global Biogeochem. Cy., 16, 1034, https://doi.org/10.1029/2001GB001448, 2002.
735 Wadsworth, F. H.: Forest management in the Luquillo mountains, I-setting, Caribbean Forester, 12, 114–124, 1951.
736 Wang, Y., Yuan, F., Yuan, F., Gu, B., Hahn, M. S., Torn, M. S., Ricciuto, D. M., Kumar, J., He, L., Zona, D.,
737 Lipson, D. L., Wagner, R., Oechel, W. C., Wullschleger, S. D., Thornton, P. E., and Xu, X.: Mechanistic modeling
738 of microtopographic impact on CH_4 processes in an Alaskan tundra ecosystem using the CLM-Microbe model, J.
739 Adv. Model. Earth Sy., 11, 4228-4304, 2019.
740 Wickham, H.: ggplot2: elegant graphics for data analysis, Springer-Verlag, New York, 2016.
741 Wood, T. E., and Silver, W. L.: Strong spatial variability in trace gas dynamics following experimental drought in a
742 humid tropical forest, Global Biogeochem. Cy., 26, https://doi.org/10.1029/2010GB004014, 2012.
743 Xu, X., Elias, D. A., Graham, D. E., Phelps, T. J., Carroll, S. L., Wullschleger, S. D., and Thornton, P. E.: A
744 microbial functional group-based module for simulating methane production and consumption: Application to an
745 incubated permafrost soil, J. Geophys. Res.-Biogeo., 120, 1315-1333, 10.1002/2015jg002935, 2015.
746 Xu, X. F., Tian, H. Q., Zhang, C., Liu, M. L., Ren, W., Chen, G. S., Lu, C. Q., and Bruhwiler, L.: Attribution of
747 spatial and temporal variations in terrestrial methane flux over North America, Biogeosciences, 7, 3637-3655,
748 10.5194/bg-7-3637-2010, 2010.
749 Xu, X., Yuan, F., Hanson, P. J., Wullschleger, S. D., Thornton, P. E., Riley, W. J., Song, X., Graham, D. E., Song,
750 C., and Tian, H.: Reviews and syntheses: Four decades of modeling methane cycling in terrestrial ecosystems,
751 Biogeosciences, 13, 3735-3755, 10.5194/bg-13-3735-2016, 2016.
752 Zheng, J., Thornton, P. E., Painter, S. L., Gu, B., Wullschleger, S. D., and Graham, D. E.: Modeling anaerobic soil
753 organic carbon decomposition in Arctic polygon tundra: insights into soil geochemical influences on carbon
754 mineralization, Biogeosciences, 16, 663-680, 10.5194/bg-16-663-2019, 2019.
755

756 **Table 1: Fitted values of M3D-DAMM model parameters.**

Parameters	Fitted values	Description	Unit	Source
GrowR$_{H2Methanogens}$	0.31		1/day	Servais et al., 1985
GrowR$_{AceMethanogens}$	1.59	Growth rates	1/day	Servais et al., 1985
GrowR$_{Methanotrophs}$	0.12		1/day	Servais et al., 1985
DeadR$_{H2Methanogens}$	0.03		1/day	Servais et al., 1985
DeadR$_{AceMethanogens}$	0.54	Death rates	1/day	Servais et al., 1985
DeadR$_{Methanotrophs}$	0.008		1/day	Servais et al., 1985
Efficiency$_{H2Methanogens}$	0.2	Substrate	unitless	Grant, 1998
Efficiency$_{AceMethanogens}$	0.04	use	unitless	Kettunen et al., 2003
Efficiency$_{Methanotrophs}$	0.4	efficiencies	unitless	Kettunen et al., 2003
KM$_{Ace}$	16		mmol/m3	Grant, 1998; McGill et al., 1981
KM$_{H2ProdAce}$	11		µmol/m3	Conrad, 1989
KM$_{H2ProdCH4}$	2.14×10^{-5}		mmol/m3	Fennell and Gossett, 1998
KM$_{CO2ProdCH4}$	9.08×10^{-9}	Half-saturation	mmol/m3	Stoichiometry theory
KM$_{CH4ProdAce}$	13	constants	mmol/m3	Kettunen et al., 2003
KM$_{CH4ProdO2}$	0.03		mmol/m3	Kettunen et al., 2003
KM$_{CH4OxidCH4}$	0.06		mmol/l	Kettunen et al., 2003
KM$_{CH4OxidO2}$	0.74		mmol/l	Kettunen et al., 2003
ACmax$_{AceProd}$	0.52	Maximum	mmol/m3/h	Smith and Mah, 1966
Acemax$_{H2Prod}$	1.31	reaction rates	mmol acetate/g/h	Conrad, 1989
rCH4Prod	0.84	Rate	mol CH$_4$/mol acetate	Kettunen et al., 2003
rCH4Oxid	3.06	constants	mol O$_2$/mol CH$_4$	Kettunen et al., 2003
Q$_{10ACMin}$	1.16		unitless	Segers, 1998
Q$_{10AceProd}$	1.21		unitless	Atlas and Bartha, 1987; Kettunen, 2003; Van Hulzen et al., 1999
Q$_{10H2CH4Prod}$	1.27	Temperature	unitless	Segers, 1998
Q$_{10CH4Prod}$	1.13	sensitivities	unitless	Kettunen et al., 2003
Q$_{10CH4Oxid}$	1.18		unitless	Kettunen et al., 2003

757

758 Initial values of model parameters were collected from literature ("Source"). Also see Xu et al. (2015) for detailed information
759 on model parameters.

760

761
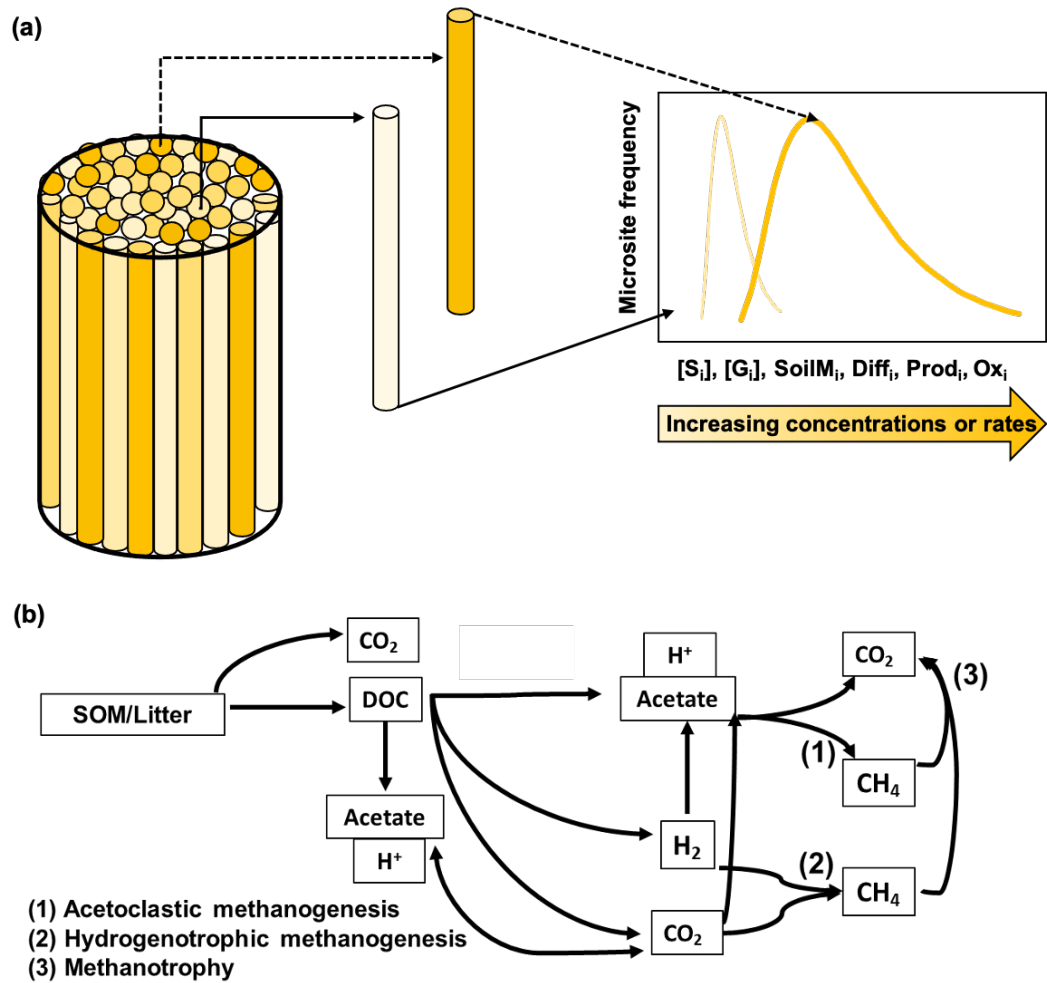
Figure 1: Conceptual figure of the modelling approach. Top panel (a) Top panel (a) shows the model representation of soil microsite distribution (modified from Sihi et al., 2020a, also see Eq. 14). The cylinder refers to the volume beneath the soil chambers. The intensity of different cylinder colors figure refers to rate of a process or the intensity of a concentration inside microsites in each theoretical cylinder, e.g., a dark color means a higher rate/intensity, and a light color means a lower rate/intensity for a given process. The 2D graph on the right refers to the probability density function of the rate of the process or intensity of the concentration in the bulk soil. A wide distribution skewed to the right (dark line) implies higher bulk rates of the process or higher concentrations, and a narrow distribution skewed to the left (light line) implies lower bulk rates of the process or lower concentrations, of any of the following: solute concentration $[S_i]$, gas concentration $[G_i]$, soil moisture ($SoilM_i$), gas and solute diffusion ($Diff_i$), methane production ($Prod_i$), and methane oxidation (Ox_i). Bottom panel (b) is the schematic of the microbial functional group-based model for simulating soil methane (CH_4) dynamics in field soils (modified from Xu et al., 2015). The schematic represents the decomposition of soil organic matter (SOM) and plant litter into carbon dioxide (CO_2) and dissolved organic matter (DOC); the production of acetate and hydronium ion (H^+) from decomposition and fermentation of DOC which also decreases pH, the production of acetate and hydronium ion (H^+) from homoacetogenesis which decreases pH; and the production of dihydrogen ion (H_2) and CO_2 from decomposition of DOC. The intermediary products then have three possible non-mutually exclusive pathways (1) aceticlastic methanogenesis, which is the production of methane from aqueous acetate found in soil solutions, (2) hydrogenotrophic methanogenesis, which is the production of methane from hydrogen, and (3) methanotrophy, which is the oxidation of methane into carbon dioxide.

779
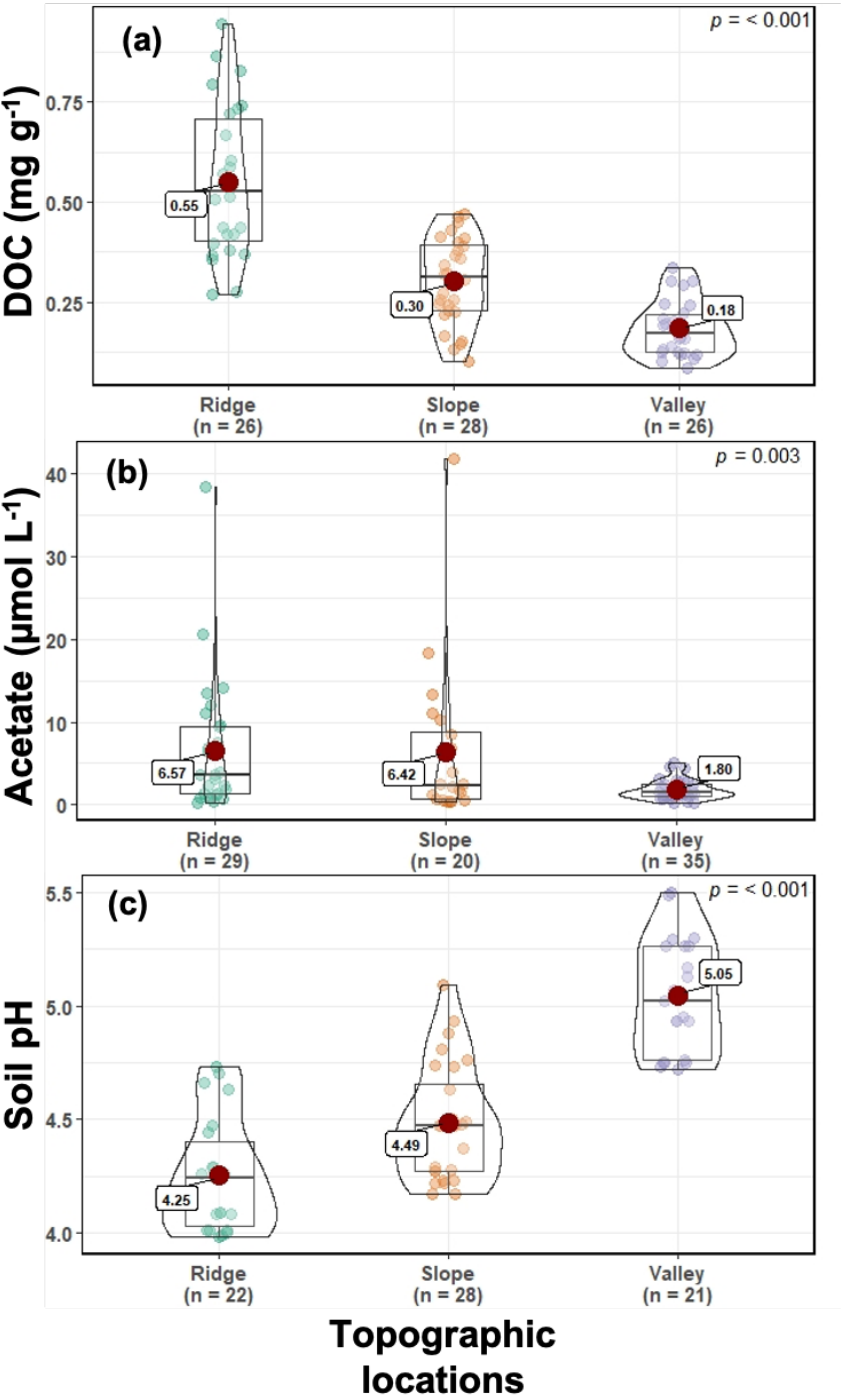
780
781 **Figure 2: Soil and porewater chemistry (dissolved organic carbon [DOC] (a), acetate (b), and pH (c)) along the ridge-slope-**
782 **valley topographic gradient.**
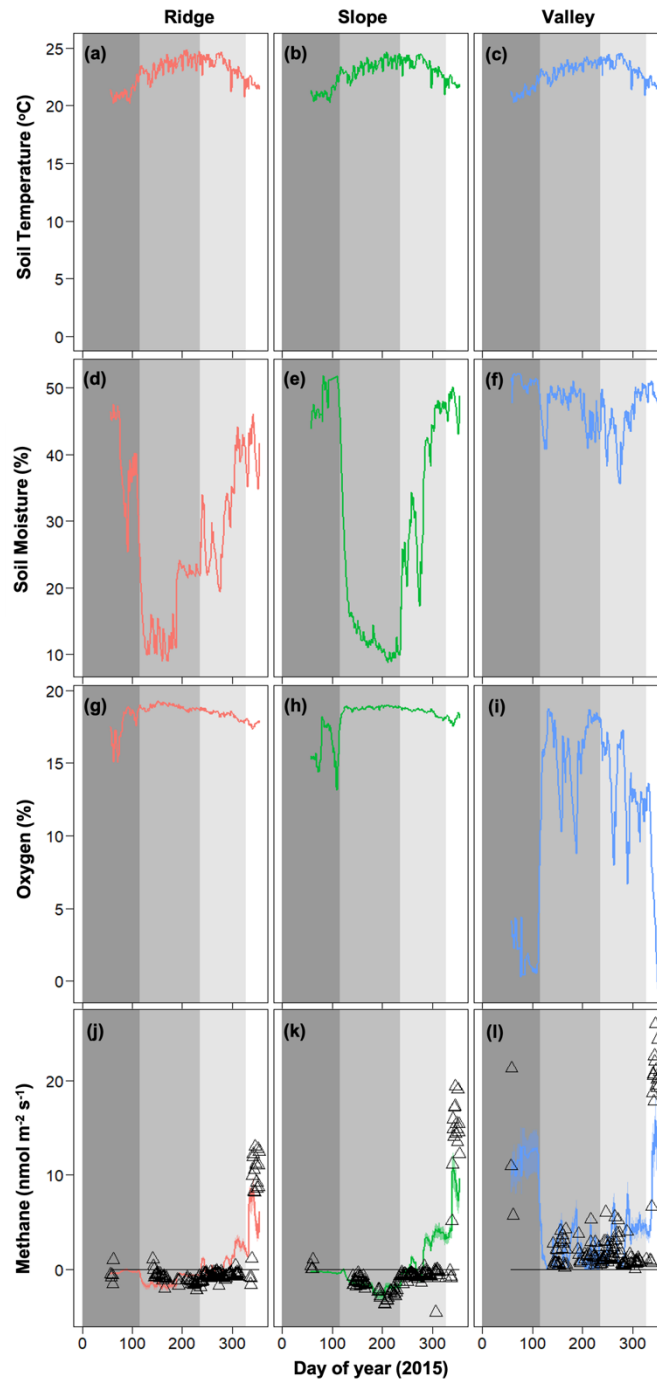
783
784   **Figure 3: Temporal dynamics of observed meteorological drivers (soil temperature (a-c), soil moisture (d-f), soil oxygen**
785   **(g-i)) and net methane emissions (j-l) for 2015 (Data are taken from O'Connell et al., 2018). For methane emissions,**
786   **symbols represent observed data and lines represent model simulations. Dark gray, medium gray, light gray, and white**
787   **shading represent pre-drought, drought, drought recovery, and post drought events (O'Connell et al., 2018).**
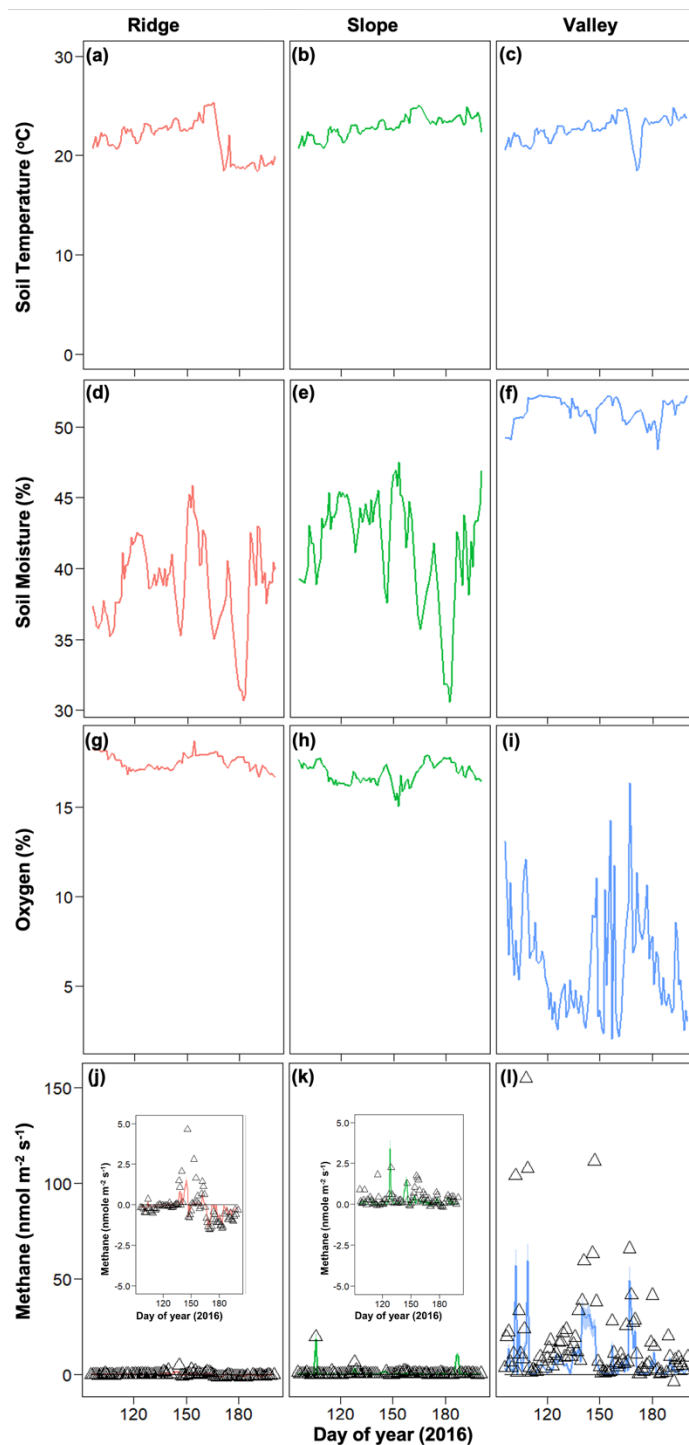
788
789 **Figure 4: Temporal dynamics of observed meteorological drivers (soil temperature (a-c), soil moisture (d-f), soil oxygen (g-
790 i)) and net methane emissions (j-l) for 2016. For methane emissions, symbols represent observed data and lines represent
791 model simulations.**

Figure 5: Relation between soil meteorology and methane emissions for 2015 (a) and 2016 (b). SoilM, SoilT, O$_2$, CH$_4$ represent soil moisture, soil temperature, oxygen, and methane, respectively. Numbers represent adjusted Holm correlation coefficients, and numbers with "X" indicate a non-significant correlation at p < 0.05.
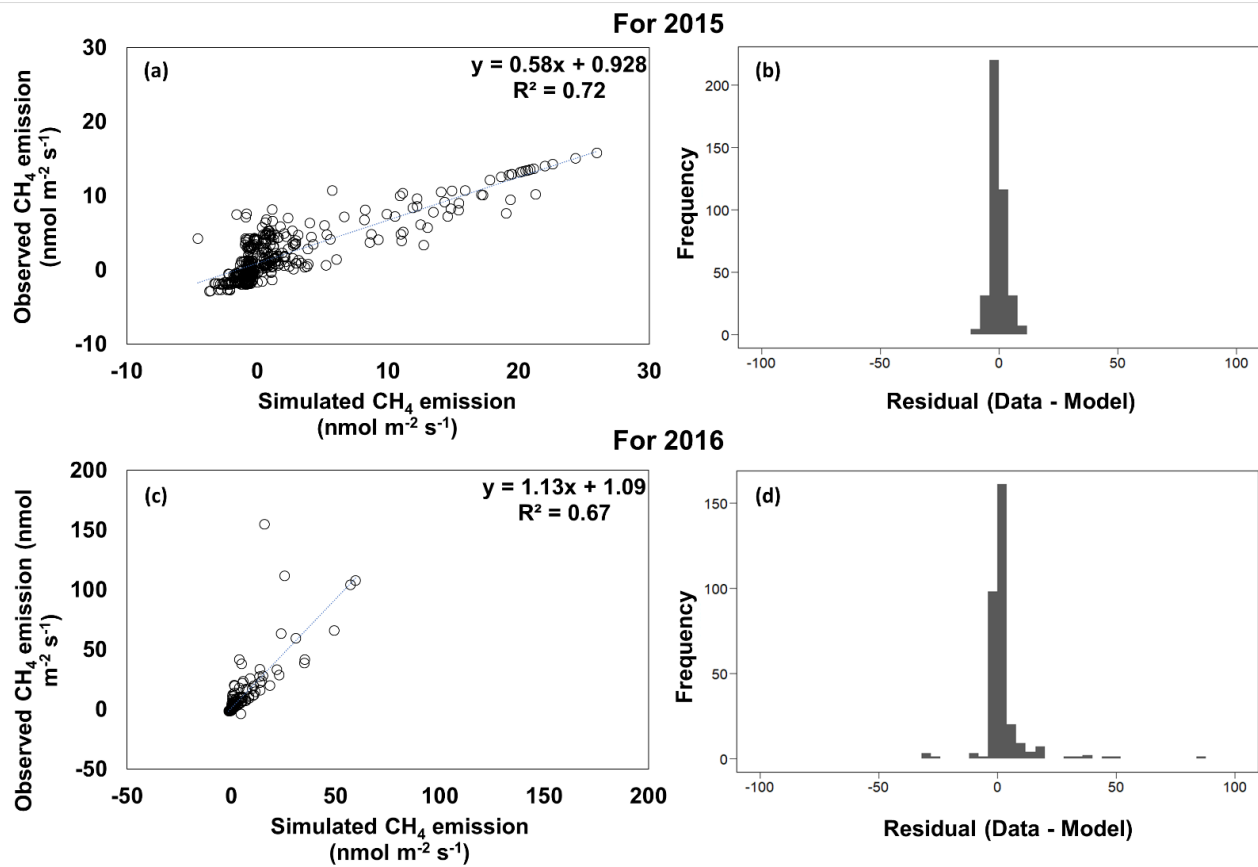
Figure 6: Observed versus simulated methane (CH₄) emissions and model residuals for 2015 (a, b) and 2016 (c, d).
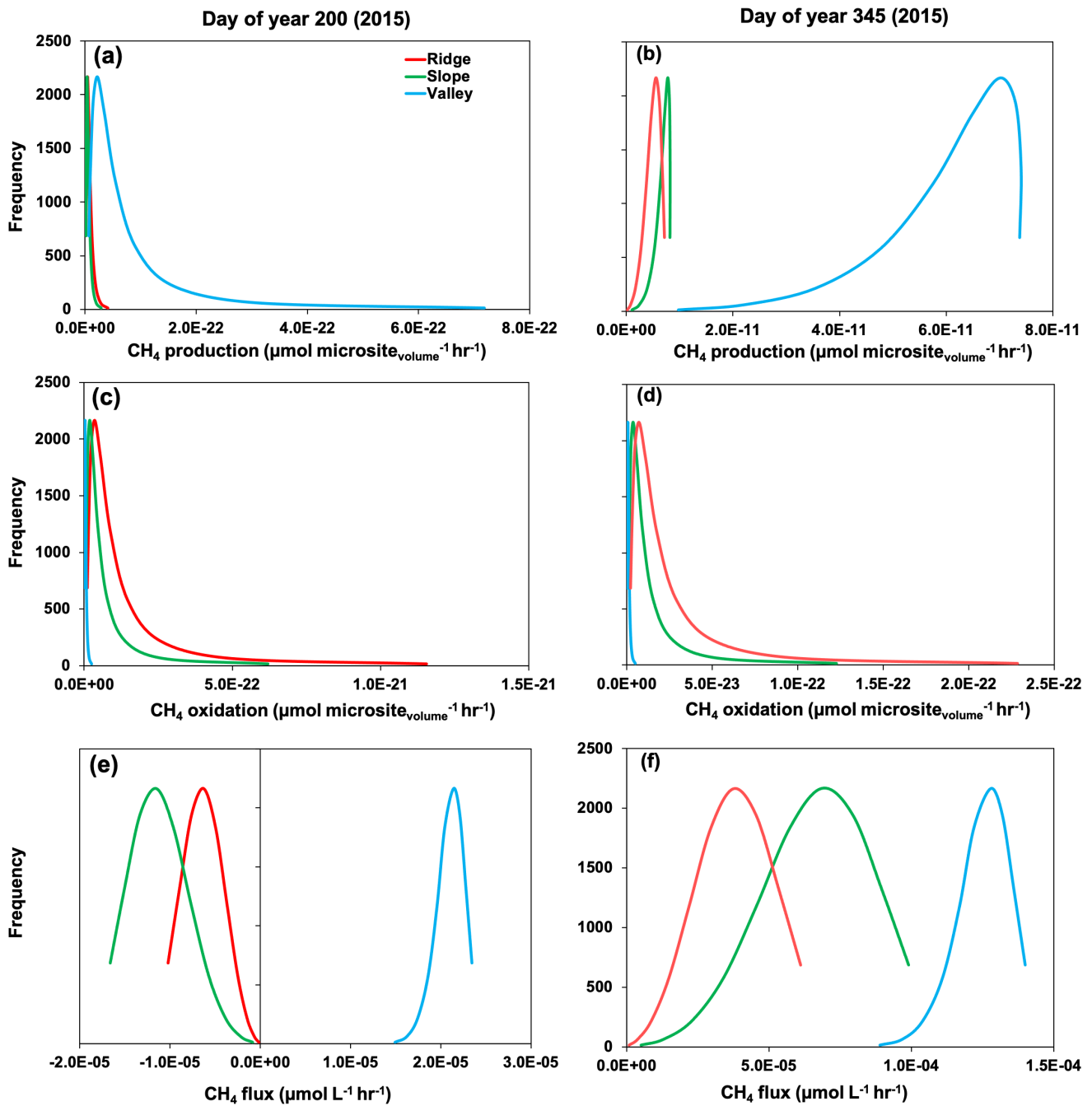
Figure 7: Rates of gross methane (CH₄) production (a, b), oxidation (c, d), and net flux (e, f) across simulated soil microsites. Day of year 200 and 345 represent drought and post-drought recovery, respectively (see medium gray and white shading in Fig. 3).
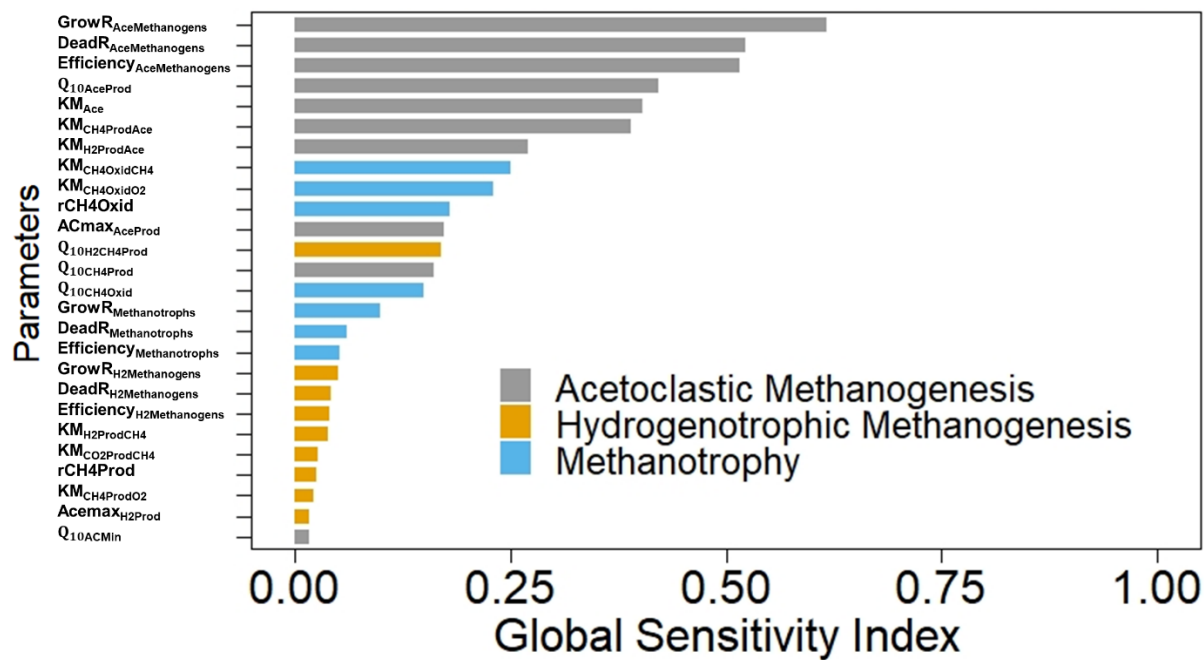
Figure 8: Global sensitivity indices of M3D-DAMM model parameters (defined in Table 1). Gray, yellow, and blue colors represent parameters for aceticlastic methanogenesis, hydrogenotrophic methanogenesis, and methanotrophy, respectively.